

## Evolution of Pleistocene travertine depositional system from terraced slope to fissure-ridge in a mixed travertine-alluvial succession (Jebel El Mida, Gafsa, southern Tunisia)

Mohsen Henchiri, Walid Ben Ahmed, Andrea Brogi, Mehmet Cihat Alçiçek & Ramdhane Benassi

To cite this article: Mohsen Henchiri, Walid Ben Ahmed, Andrea Brogi, Mehmet Cihat Alçiçek & Ramdhane Benassi (2017) Evolution of Pleistocene travertine depositional system from terraced slope to fissure-ridge in a mixed travertine-alluvial succession (Jebel El Mida, Gafsa, southern Tunisia), *Geodinamica Acta*, 29:1, 20-41, DOI: [10.1080/09853111.2016.1265398](https://doi.org/10.1080/09853111.2016.1265398)

To link to this article: <https://doi.org/10.1080/09853111.2016.1265398>



© 2017 The Author(s). Published by Informa UK Limited, trading as Taylor & Francis Group



Published online: 12 Dec 2016.



[Submit your article to this journal](#)



Article views: 1054



[View related articles](#)




[View Crossmark data](#)



Citing articles: 7 [View citing articles](#)



## Evolution of Pleistocene travertine depositional system from terraced slope to fissure-ridge in a mixed travertine-alluvial succession (Jebel El Mida, Gafsa, southern Tunisia)

Mohsen Henchiri<sup>a\*</sup> , Walid Ben Ahmed<sup>a</sup>, Andrea Brogi<sup>b</sup> , Mehmet Cihat Alçiçek<sup>c</sup>  and Ramdhane Benassi<sup>a</sup>

<sup>a</sup>Department of Geology, Gafsa University, Sidi Ahmed Zarrouk 2112, Gafsa, Tunisia; <sup>b</sup>Department of Earth and Geoenvironmental Sciences, University of Bari “Aldo Moro”, Bari 70125, Italy; <sup>c</sup>Department of Geology, Pamukkale University, Denizli 20070, Turkey

(Received 22 May 2016; accepted 23 November 2016)

The Quaternary stratigraphic record of Jebel El Mida, composed of continental deposits, is a useful example of concomitant travertines and alluvial deposition in an extensional setting. Travertine deposition occurred in a faulted Pleistocene alluvial fan giving rise to seven (recognised) facies interfingering with five other alluvial ones. The travertine depositional events indicate a tectonically driven evolution from terraced slope (facies group FC1–FC6) to a travertine fissure ridge-type depositing phase (facies group of FC1–FC7). Interfingering between travertine and alluvial facies indicates the co-existence of adjacent and time-equivalent depositional environments. The travertine deposition resulted from deep origin hydrothermal fluids channelled along damaged rocks volumes associated to a regional fault system, named as the Gafsa Fault (GF). The travertine–terrestrial succession in Jebel El Mida highlights the major role played by the GF in controlling: (i) the hydrothermal fluid flow, still active as also indicated by the numerous thermal springs aligned along the fault zone; (ii) paleoflow directions, discharge locations, volume, rate and fluctuations of the water supply. The paleoclimatic correlation with adjacent localities reveals that, at that time, humid episodes could have contributed to the recharge of the hydrothermal system and to the deposition of alluvial sediments.

**Keywords:** travertine; alluvium; depositional system evolution; Pleistocene, Tunisia

### 1. Introduction

Travertine is a thermogene continental carbonate deposit associated with thermal springs, and whose deposition is induced by CO<sub>2</sub> outgassing favoured by the fluids' pressure drop, turbulence of running water and microbial activity (Pentecost, 2005). Travertine deposits are relevant in providing helpful elements (i.e. paleoclimate, paleoecology of the spring system, tectonic setting, paleohydrology, paleotopography and thermal history) for geological reconstruction (Brogi, Capezzuoli, Aqué, Branca, & Voltaggio, 2010; Brogi et al., 2016; Chafetz & Folk, 1984; Ford & Pedley, 1996; Gandin & Capezzuoli, 2008; Guo & Riding, 1999; Pentecost, 2005). The term travertine is used to indicate a variety of deposits associated with thermal (generally > 30 °C) and HCO<sub>3</sub>-enriched (>7 mmol/l) springs through mostly abiotic depositional processes (Gandin & Capezzuoli, 2014). The travertine mineralogical composition is dominated by calcite and/or aragonite (dendritic, blades and acicular crystals) with higher (cm to m/year) sedimentation rates of regularly bedded to finely laminated fabrics (Chafetz & Folk, 1984; Pentecost, 2005). The depositional morphologies include multi-symmetrical bodies such as mounds, slopes and ridges (Gandin & Capezzuoli, 2014). They are distinguished from tufa by the abundance of coated gas bubbles and shrub lithofacies (Guo & Riding, 1999). The hydrological setting of travertine deposits is dominated by regular and permanent flow hydrodynamics with a strict relationship

to tectonics (Hancock, Chalmers, Altunel, & Çakir, 1999). The travertine deposition is scarcely influenced by anthropogenic or climate-controlling factors (Gandin & Capezzuoli, 2014).

The term tufa is used to indicate a dominantly biotic continental carbonate associated with cool fresh water streams and springs (Ford & Pedley, 1996; Gandin & Capezzuoli, 2014; Pedley, 2009). The tufa mineralogical content is dominated by calcite (micrite and microsparite) and the absence of the aragonite. Its sedimentation rates, ranging from few mm to cm/y, are lower than those characterizing the travertine deposition. The most conspicuous character of the tufa deposits is the abundance (over 40%) of the primary porosity due to the richness of its biological content represented by micro and macrophytes (Ford & Pedley, 1996; Jones & Renaut, 2010). The depositional morphologies of tufa include axial-symmetrical bodies such as cascades, dams and barrages with a distinctive phytoherm lithofacies. Tufa deposition is mostly controlled by climate change and deeply influenced by anthropogenic interference in its deposition system (Gandin & Capezzuoli, 2014). Although the terms travertine and tufa are used to categorize continental carbonates formed in very different environments, there are cases where travertine and tufa can deposit in the same depositional system: in fact, travertine is reported to occur in different depositional systems, including terraced slopes (Altunel & Hancock, 1993b; Capezzuoli et al., 2016),

\*Corresponding author. Email: [mohsen.henchiri@fsg.mu.tn](mailto:mohsen.henchiri@fsg.mu.tn)

waterfalls and cascades (Chafetz & Folk, 1984; Pentecost, 2005), depression fills (Guo & Riding, 1998), fissure ridges (Altunel & Hancock, 1993a; Atabey, 2002; Brogi & Capezzuoli, 2009; Brogi, Capezzuoli, Alçiçek, & Gandin, 2014; Brogi et al., 2016; De Filippis et al., 2013; Guo & Riding, 1999; Selim & Yanik, 2009) and channels (Drysdale, 1999). These depositional systems could laterally interact with different environments (i.e. fluvial or lacustrine) favouring tufa and/or lacustrine carbonate deposition interacting with terrigenous sedimentation. Description of these articulated and laterally variable depositional systems is scarce in the literature and is reported only for restricted areas (cf. Croci, Porta, & Capezzuoli, 2015; Huerta et al., 2016; Martini & Capezzuoli, 2014; Viles, Taylor, Nicoll, & Neumann, 2007).

In order to contribute to the better understanding of the sedimentary and tectonic interplay in a depositional system characterized by the interaction between travertine and alluvial terrigenous deposition, a key area exposed nearby the Gafsa city, southern Tunisia (Figure 1), has been analysed. These travertine deposits have been scarcely studied and few data have been published on their age, origin and depositional systems;

these have been considered so far as continental carbonates and described as calcretes and dolocretes (Abdeljaouad, 1991; Gallala, Gaied, Essefi, & Montacer, 2010; Regaya, 2002). Furthermore, these deposits are interlayered with alluvial sediments in a relatively wide alluvial fan system.

Recently, the travertine deposits in the eastern part of Jebel El Mida along the strike-slip GF in southern Tunisia have been documented by Henchiri (2014a). Furthermore, Jebel El Mida travertine has only been attracted for its archaeological remains encrusted in the conglomeratic level and composed of lithic flakes, hand axes, burins and scrapers assigned to late Acheulean age (Collignon, 1887; Gobert, 1952; Vaufrey, 1933).

The study of Jebel El Mida travertine allowed us to reconstruct an articulated depositional system characterized by travertine formation along with alluvial deposits in which facies changes of terraced slope to fissure ridge took place. In addition, we emphasize the interaction between travertine and alluvial terrigenous deposition in an active extensional basin, where tectonic (mainly) and climatic factors played a fundamental role in controlling the evolution of this continental succession.

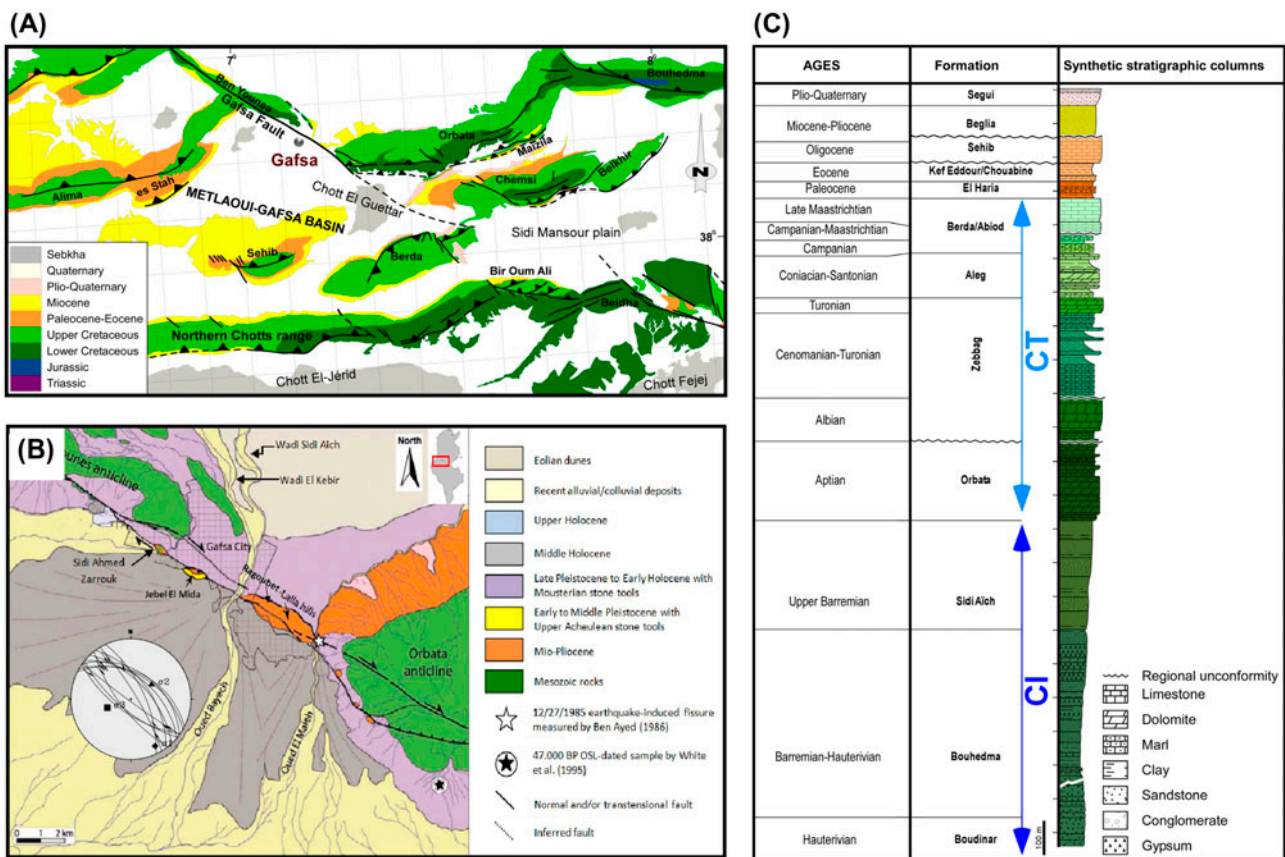


Figure 1. (A) Simplified geological map of the southern Atlas foreland in Tunisia (Gharbi et al., 2014). (B) Morphotectonic map of the Gafsa area derived from SPOT 5 satellite images analysis and field reconnaissance (Said et al., 2011). Cross-cutting striations recorded on the Gafsa Fault plane indicate the transpressional stress regime. (C) Stratigraphic column of the Mesozoic and Cenozoic series around Gafsa city showing the main hydrostratigraphic units (Gharbi et al., 2014).

## 2. Geological setting

### 2.1. Location and hydrostratigraphy

The study area is located 1 km to the south of Gafsa City within the north-west-trending ranges of southern Tunisian Atlas (Figure 1(A)). It is bordered to the north by the Gafsa Fault (hereafter GF), and covers an area of 15000 m<sup>2</sup> with a maximum altitude of 328 m. The range of daily and annual temperatures shows high seasonal variation with irregular precipitation as typical of semi-arid and arid regions. The average rainfall ranges from 100 to 250 mm/y. The drainage network consists of south-draining intermittent streams including Wadi Kabir, which join Wadi Sidi Aich at Gafsa to form Wadi Bayech.

The aquifer levels belonging to the main hydrostratigraphic units are shown in Figure 1(B). Here, the oldest aquifer unit is called ‘the continental intercalaire CI’ (Edmunds et al., 2003) and it has a potential reservoir thickness ranging from 200 to 1000 m (Castany, 1982). The CI aquifer is hosted in Lower Cretaceous continental (fluvio-deltaic) deposits, i.e. Boudinar and Sidi Aich formations, which constitute the main aquifer levels of the CI. Lithological facies of the CI-bearing formations are variable but dominated by detrital facies. The Boudinar Formation, Hauterivian to Barremian in age, comprises an alternating sequence of sandy and clayey layers with a thickness ranging from several to 60 m. The Sidi Aich Formation is composed of 50-m-thick feldspar-rich and white friable sands. The second hydrostratigraphic unit is called ‘the Continental Terminal CT’ hosted in the 1000-m-deep upper Cretaceous and Cenozoic formations (Edmunds et al., 2003). Lithologically, the CT-hosting formations are different with distinct three aquifer levels. The main level in Gafsa region is located within the carbonates and evaporates of Zebbag Formation (Upper Cenomanian) with a thickness ranging from 120 to 150 m for the dolomite and chalky levels and 300–400 m for the upper marly, clayey and gypsum horizons. The youngest aquifer unit belongs to the Mio-Pliocene Beglia and plio-Quaternary Segui formations. The Beglia Formation (Miocene – lower Pliocene) deposited in a fluvial environment, composing coarse-grained sandstone intercalated with mudstone, showing variable thickness reaching 400 m near the region of Moulares to West of Gafsa. This formation is overlain by the upper Pliocene loess bearing Segui Formation (Mannai-Tayech, 2009), consisting of clays and silts with 150–400-m-thick continental sequence, and it is considered as the base of the Quaternary sequence.

### 2.2. Tectonic outline

Southern Atlas domain of Tunisia is described as a curved, right-stepping ‘en echelon’ folds associated to the NW-trending lateral strike-slip of the GF systems (Gharbi,

Bellier, Masrouhi, & Espurt, 2014; Saïd, Chardon, Baby, & Ouali, 2011) (Figure 1(A)). The southern Tunisian Atlas is a fold and thrust belt composed of S-verging anticlines. Locally, the Metlaoui-Gafsa area is composed of E- to ENE-trending anticlines (e.g. Sehib, Berda and Orbata) and basins (e.g. El Maïzila and Sidi Mansour synclines) which interfere with the NW-trending transtensional and transpressional deep-seated GF (Boukadi, 1994; Gharbi et al., 2014; Saïd et al., 2011; Zargouni & Ruhland, 1981). The tectonic evolution of the southern Tunisian Atlas started with the reactivation of Late Cretaceous faults active during the Mesozoic and the Cenozoic (Frizon de Lamotte, Saint-Bezar, Bracene, & Mercier, 2000; Gharbi et al., 2014; Saïd et al., 2011; Zargouni & Ruhland, 1981; Zouari, Turki, & Delteil, 1990). A first Cenozoic tectonic event (Eocene), the Atlasic compressional event, was associated to a WNW- to NW-trending compression (Figure 1(C)) that caused the inversion of some major extensional Cretaceous structures (Frizon de Lamotte et al., 2000; Guiraud & Bosworth, 1997). Since late Pliocene, a N-trending compressional tectonics (Saïd et al., 2011) was producing thrusts through the reactivation of Mesozoic normal faults (Gharbi et al., 2014; Saïd et al., 2011).

The GF was generally assumed to be an inherited structure from the Mesozoic rifting of the southern Tethyan margin (Gharbi et al., 2014). The middle segment of the GF represents the oldest portion of the stratigraphic succession and consists of Triassic evaporites cropping out along the major fault. These units were locally over thrust on younger successions along NW–SE and E–W-trending right-lateral oblique-slip faults (Hlaiem, 1999). Nevertheless, the GF fault is still active as testified by numerous earthquakes occurring in the Gafsa region (Figure 1(C)). Here, the seismically active zones are concentrated along the major N140° strike-slip fault. Instrumental seismological data show that almost 50 seismic events were recorded nearby the GF since 1975; the majority of them (30) have  $M > 3$  with the strongest instrumental record during 12/27/1985 (Ben Ayed, 1986). Kinematic data collected in this study indicate a transpressional movement (Figure 1(C)) compatible with the regional kinematic regime detected in several previous studies (Gharbi et al., 2014). Nevertheless, on the northwest-dipping fault scarp affecting Pleistocene alluvial deposits (about 150-m long, 1–6-m high and trends 115° and dips about 70° NE) (Figure 2(A)), superposed kinematics indicators have been recognised, revealing a composite kinematics. The kinematic indicators consist of mechanical striations on the slip surface (Figure 2(B)–(E)) suggests a first activity characterised by a down-dip movement; sub-horizontal striations are superimposed on the down-dip indicators, therefore suggesting a strike-slip kinematics (Figure 2(G) and (H)) accompanying the later evolution of the fault.

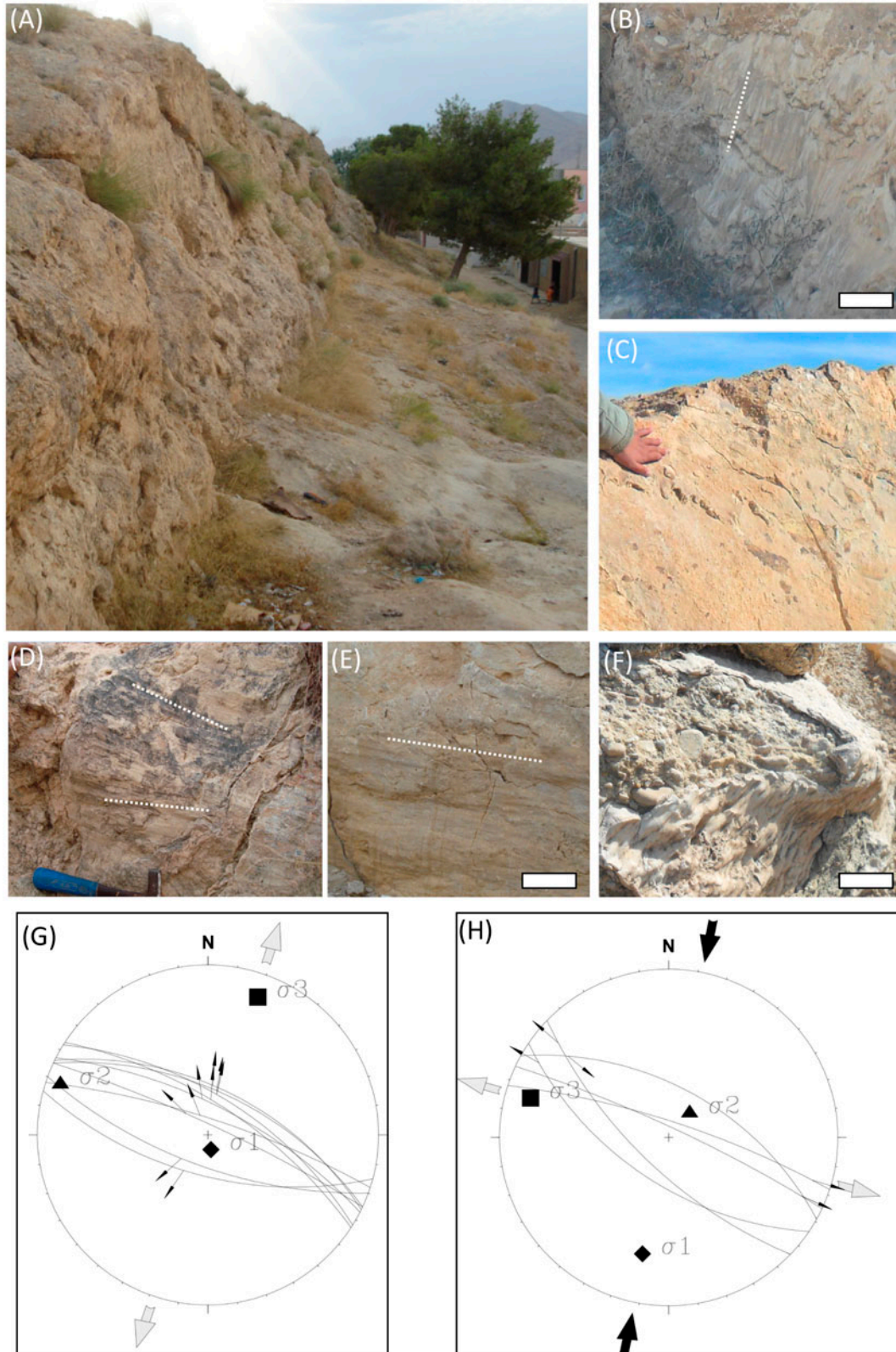


Figure 2. (A) Well-defined linear north-west-facing scarp about 150-m long, 1–6-m high and trends  $115^\circ$  and dips about  $70^\circ$  NE. (B) Kinematic indicators mainly consist of mechanical striation (scale bar = 20 cm). (C) Mineralised fault plane, Fe hydroxides and carbonates forming millimetre-thick crusts on the fault plane. (D) and (E) kinematic indicators consisting of sub-horizontal mechanical striation. (F) Heavy travertine incrustation of high-angle intersected fracture planes (scale bar 10 cm). (G) and (H) Stereographic diagrams (lower hemisphere, Schmidt diagram) of the kinematic data collected for the strike-slip faults indicating cross-cutting striations recorded on the fault plane indicate two distinct slip generations and thus two distinct stress regimes along the Jebel El Mida structure.

### 3. Material and methods

Restricted by the exposure of the travertine–terrigenous succession in the field (Figure 4(A)), six representative sections were logged and described (Figure 4(B)) in which sedimentary structures, lithologic components, stratigraphic relationships and geometry of the rock strata were recorded in detail in order to define the fabric types, their lateral and vertical multi-scale variations and the depositional processes governing their deposition and the environment in which they were deposited.

Field and satellite photographs of an area approximately 12-km wide and comprehending the water gap between the Jebels (ranges) of Ben Younes and Orbata have been analysed in order to identify the sites of measurement of stratigraphic section and determine geomorphic features to characterise the geometry and kinematics of the Major Fault (GF).

The stratigraphic sections have been chosen on the basis of their stratigraphic position, structural features, exposure and accessibility. Each section was described, sampled and photographed in the field. Sections were sampled at 0.1 m intervals depending on the nature of the stratigraphic section and travertine content. Travertine and terrigenous detrital samples were sampled in the field for the preparation of thin sections and polished (travertine) rock slabs and the results were used to identify grain, matrix and cement percentage to aid in rock classification. Grain size estimates, discriminated in the field, were made with a visual grain size chart based upon the Wentworth scale (1922). Re-examination of representative samples in the laboratory with binocular microscope confirmed the general accuracy of the field determinations.

The mineralogical composition and the low-Mg chemical character of the travertines were carried out with an X-ray powder GBC diffractometer with Cu-K $\alpha$  X-ray radiation at an accelerating voltage of 40 kV and electrical current of 20 mA, and Bruker Vector 22-based FTIR spectroscopy, respectively.

### 4. Lithofacies

First attempt on the definition of the tufa and the travertine in Gafsa region has been made by Henchiri (2014a), in which the entire architecture of the depositional units was not clearly defined (e.g. fissure ridge). In this work, and owing to a more clear vision of the deposits comprising both terraced slope and fissure ridge, morphologies have been described as travertine rather than tufa. Two travertine outcrops were recognised in Jebel El Mida. The first corresponds to remnants of terraced slope travertine in the western part of Jebel El Mida (Figure 3(C) and (D)), whereas the second, in the eastern part, consists of relatively preserved fissure ridge travertine (Figure 3(A), (B) and (E)). This latter, even though faulted and uplifted, it is still recognisable as well its entire morphology. The exposure of the studied

succession in the field (Figure 3(F)) has permitted the description of six representative sections (Figure 3(G)). Seven travertine lithofacies (Table 1) were identified and analysed according to their fabric multi-scale characteristics. Their facies code and description were based on the terminology proposed by Chafetz and Folk (1984), Guo and Riding (1998), Jones and Renaut (2010) and Croci et al. (2015). Granular travertine lithofacies were classified according to the scheme of Dunham (1962). Floatstone refers when 10% of the particles are larger than 2 mm with matrix support and rudstone refers clast-supporting (Embry & Klovan, 1971). The ‘boundstone’ terminology was ascribed to certain travertine lithofacies with rigid micritic framework. Five alluvial fan lithofacies have been distinguished (Table 2).

#### 4.1. Dentritic boundstone (FC1)

##### 4.1.1. Description

These facies consist of shrub-like and spherical structures (Figure 4(A) and (B)) composed of dentritic peloidal micrite nucleating and flouring either planar or undulated exposed surfaces developed on various substrates. They exhibit diverse branching and clumping morphologies ranging from upward expanding small rounded knobs (0.2–1.5 cm high) to domal lobes (1–3 cm high) that grew and draped pre-existent substrates represented by laminated boundstone, rafts and reed boundstone. In thin section (Figure 4(C)), the shrubs show irregular branching morphologies with discernible radiating and arborescent appearance.

##### 4.1.2. Interpretation

The dentritic shrub boundstone is interpreted as bacterial in origin (Chafetz & Guidry, 1999). The development is restricted to chemically harsh, hot-water travertine deposits in terrace pools, depressions and fissure ridge (Chafetz & Guidry, 1999) and their morphologies are strongly influenced by the bacterial colonies (Chafetz & Folk, 1984; Chafetz & Guidry, 1999; Chafetz & Meredith, 1983). However, such carbonate constituents have been ascribed to abiogenic precipitation processes by Pentecost (2005).

#### 4.2. Laminated boundstone (FC2)

##### 4.2.1. Description

These facies are represented by alternation of banded porous laminated boundstone composed of micrite and microsparite and dense laminated boundstone composed of dense micrite (Figure 4(D), (E) and (G)). The number and the thickness of these laminae are variable, ranging from 6 to 30 generations of 0.5–1-cm-thick laminae. The shape and microstructure of these laminated boundstones range from planar to drib lobe-like laminated structures (Figure 4(F)) to crenulated forms exhibiting sometimes

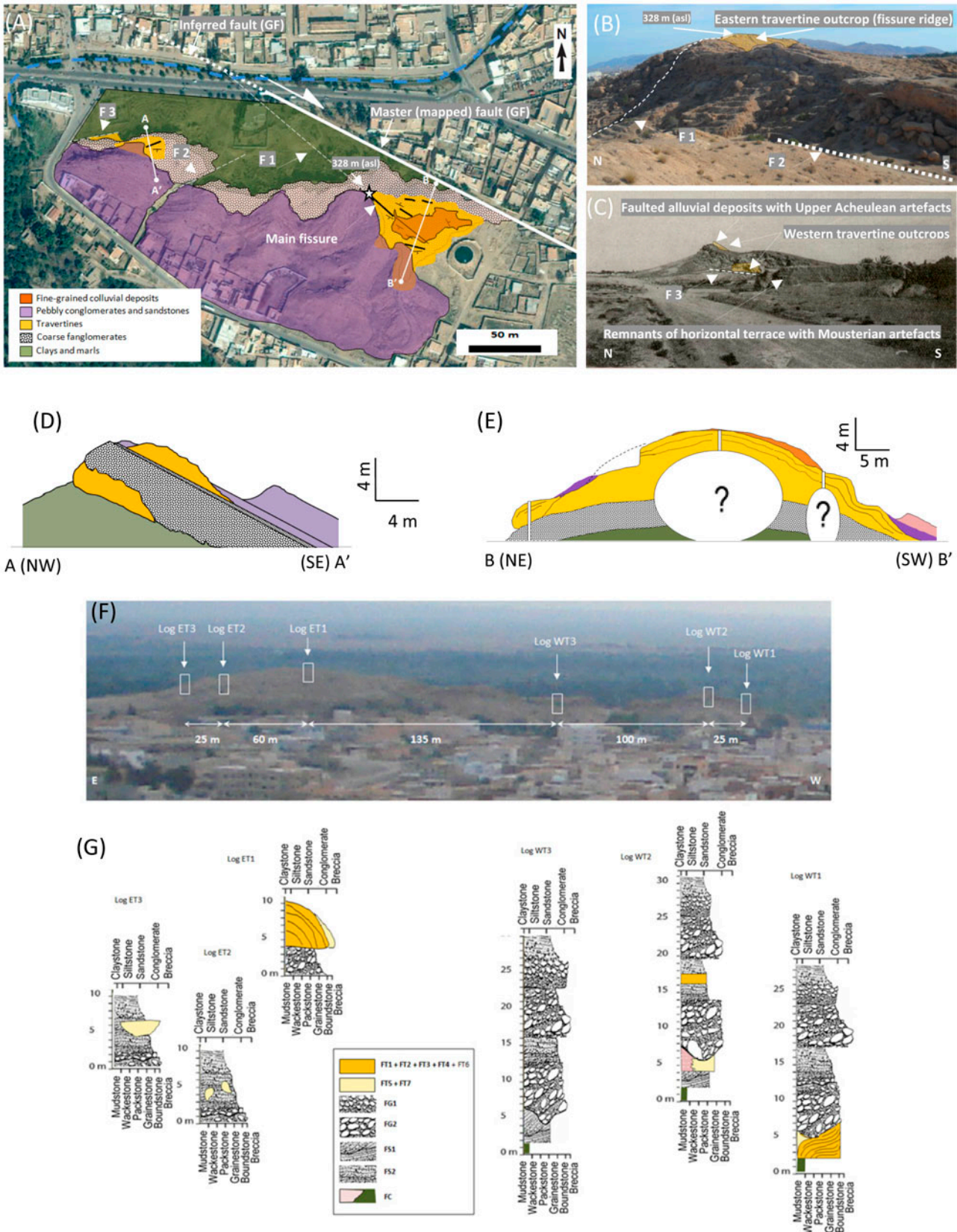


Figure 3. (A) Simplified map of Jebel El Mida structure showing the main travertine outcrops and the mapped and the inferred faults. (B) The travertines of the eastern compartment of Jebel El Mida. (C) The travertines of the western compartment of Jebel El Mida. (D) The A–A’ cross-section in (A). (E) The cross-section of B–B’ in (A). (F) Panoramic view of the exposed succession in the structure of Jebel El Mida showing the location of the measured stratigraphic logs. (G) The stratigraphic logs with lithofacies grouped into lithofacies associations.

Table 1. Description and interpretation of travertine lithofacies identified in the succession of Jebel El Mida.

| Facies                                       | Thickness       | Lateral continuity               | Morphology   | Composition   | Interpretation   |
|--|-----------------|----------------------------------|--|---|--|
| FC1: Dentritic boundstone                    | 1 to 3 cm       | Up to 50 cm                      | Small rounded knobs to domal lobes, irregular shrub branching, discernible arborescent appearance                      | Dentritic peloidal micrite  | Bacterially mediated and restricted to hot water terraced slope or fissure ridge travertines   |
| FC2: Laminated boundstone                    | 2 mm up to 3 cm | 1 to 50 cm                       | Planar to crenulated forms, occasionally broken and disrupted with corrugation and undulation                          | Dense laminae beige to light grey in colour, the number and the thickness of these laminae are variable, ranging from 6 to 30 generations of laminae and 2 microns to 1 cm in thickness | Encountered in the spring thermal pools of either terraced slope or fissure ridge depositing systems or in the poorly drained portions of the spring |
| FC3: Raft boundstone/<br>rudstone            | 5 to 10 cm      | Fragmented or 5- to 50-cm sheets | Lenses of thin flat to wavy film structures  | Densely packed sheets of carbonate films preserving locally intra-raft porosity   | Occurrence in the surface of stagnant waters in pond systems and pools of terraced slope and fissure ridge systems                                   |
| FC4: Coated bubble boundstone                | 3 cm            | 10 cm to 1 m                     | Isolated bubbles or honeycomb structure  | Thin layers of micrite ranging from 10 to 30 µm in thickness encasing hollow space, the inner wall of the lithified bubble is lined by scalenohedral sparite cement                     | Occurrence on the planar surfaces of ponds and pools of terraced slopes with slowly flowing laminated waters   |
| FC5: Reed boundstone/<br>rudstone/grainstone | 50 cm           | Up to 10 m                       | Original upright position or horizontally crowded  | Trunk and stem and branch moulds and leaf imprints, composed of alternating laminae of porous and dense micrite. Number of laminae ranges from 6 to 8, thickness is from 2 to 3 mm      | Encountered in the relatively distal sites and absent in the vicinity of the ridge fissures or spring vents  |
| FC6: Coated grains                           | 10 to 100 cm    | Up to 5 m                        | Densely packed sheets with no preferential orientation filling pre-existing topographic irregularities and depressions | Grams with a nucleus coated by cortical laminae, size from 0.5 to 3 cm in diameter, lamina couplets of dense dark and porous light micrite  | Bacterially mediated in pools that periodically agitate  |
| FC7: Insect larval tube boundstone           | 5 cm            | Up to 10 m                       | Individual tubes oriented normal to bedding, roughly parallel to each other only upper ends of the tubes are open      | Calcified cylindrical tubes, inner tube walls are lined with 0.1- to 0.5-mm-thick beige to white dense micrite ring   | Pyralid insect larval tubes (burrows) built in gently flowing water over the travertine masses   |



Table 2. Description and interpretation of alluvial lithofacies identified in the succession of Jebel El Mida.

| Facies   | Description  | Interpretation  |
|--|--|---|
| FT1: Disorganised matrix-supported conglomerates           | Matrix-supported sub-angular to sub-rounded and poorly sorted cobble-boulder clasts, clast size ranging from several cms to 1 m, crude imbrications are common, thickness ranging from 0.5 m to 2 m, matrix consisting of detrital terrigenous silty sand and mud and locally structureless micrite and microsparite | Poorly sorted, muddy matrix-supported gravel. Chaotic fabric is interpreted as a deposition by cohesive clast-rich debris flow, remobilisation of debris flow by water action is evidenced by the presence of crude stratified gravel |
| FT2: Disorganised matrix- to clast-supported conglomerates | Disorganised, poorly sorted, ungraded and matrix- to clast-supported pebble, cobble to boulder clasts, clast size varies from few cms to 80 cm, bedding thickness averages between 20 and 60 cm, irregular basal contacts, coarse sand-granule matrix.   | Deposition by hyperconcentrated flood flow triggered by catastrophic flood events and/or heavy rainfall   |
| FTS1: Stratified sandstones                                | Trough to normally graded cross-stratifications, erosive upper contacts, and low-angle cross-strata from 15 to 25°, passes upward and laterally into more massive and/or pink-coloured planar and laminated sandstones   | Rapid deposition under waning stage of alluvial channel or by other low-magnitude flow  |
| FTS2: Massive sandstones                                   | Fine to very fine reddish pink to brown-coloured moderately consolidated massive sandstones, lateral discontinuity and thickness varies between 50 cm and 1 m, erosive contacts with overlying beds, presence of prehistoric flint stone tools   | Sedimentation through gravity flow in shallow water restraining bedform development. Locally, they can represent the conglomeratic bar surface deposits in the overbank areas of an alluvial plain                                    |
| FT3: Massive mudstones                                     | Green, reddish brown to yellow-coloured massive (to slightly laminated) and thick-bedded siltstones and claystones, irregular contacts with overlaying beds  | Over bank deposits associated with the paleosol and pedogenic carbonate development   |

broken and disrupted laminae with corrugation and undulation where laminae do not exactly match each other. Dense laminated boundstones consist of dense laminae of beige to light grey in colour. Layers of laminated boundstone average from 2 mm up to 1 cm in thickness and locally disrupted by isolate sub-spherical to lenticular 3-mm–1-cm-wide pores (Figure 4(D)).

#### 4.2.2. Interpretation

These lithofacies are encountered in the spring thermal pools of either terraced slope or fissure ridge depositing systems or in the poorly drained portions of the spring (Ford & Pedley, 1996; Pentecost, 2005). It is ubiquitous as demonstrated in modern travertine depositing systems such as those in Rapolano Terme in Italy (Brogi & Capezzuoli, 2009; Chafetz & Folk, 1984; Guo & Riding, 1998) and in the Denizli basin in Turkey (Altunel & Hancock 1993a; De Filippis et al., 2013; Khatib et al., 2014), where cyanobacteria with their associated biofilms contribute to the development of laminae by acting as substrate for the calcite nucleation and the fixation of the CaCO<sub>3</sub> grains. In addition, the laminated structure can indicate periods of stability of their support, which once moved can lead to the disruption and the breaking of the laminae. The alternation of laminae and the variability of crystal shape are attributed to seasonal fluctuations of the spring water temperature, chemistry and flowing regime (Andrews & Brasier, 2005; Chafetz, Rush, & Utech, 1991).

### 4.3. Raft boundstone/rudstone (FC3)

#### 4.3.1. Description

These facies consist of few microns to 3-mm-thick white to beige colour (Figure 4(H)) deposits. Their morphology varies from flat to wavy depending upon the morphology of their substrate. They range from widely to densely packed sheets of carbonate films preserving locally intra-raft porosity. The fragmented and re-sedimented raft fragments often develop cemented grainstone/rudstone lenses ranging in thickness from 5 to 10 cm and with lateral extension varying from 1 to several metres. Raft boundstone often serves as a precipitation support for shrub boundstone.

#### 4.3.2. Interpretation

Raft sheets and fragments are interpreted as being the result of calcite or aragonite precipitation in the surface of stagnant waters belonging to pond systems and pools of terraced slope and fissure ridge systems (Guo & Riding, 1998). Some authors ascribed them to ponds near the hydrothermal vents (Folk, Chafetz, & Tiezzi, 1985; Jones & Renaut, 2008). The development of raft grainstone/rudstone to floatstone is triggered by various mechanisms. The continuous growth of calcite or aragonite crystals in the upper and lower raft surfaces increases the density of rafts that collapse and sink to the bottom of the pool. Stagnant waters are the main condition for the raft precipitation which explains why

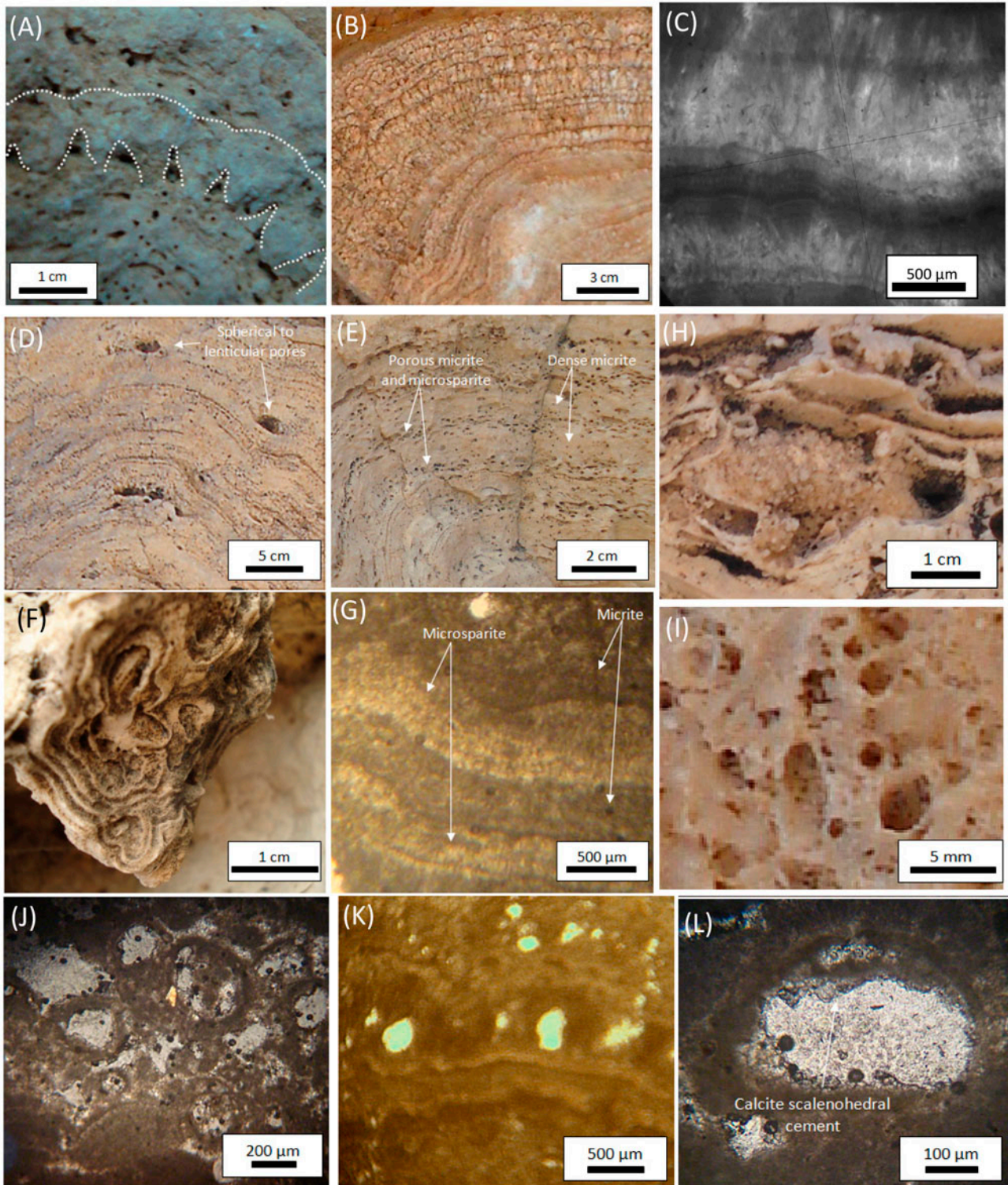


Figure 4. (A) Arborescent shrub-like morphology. (B) Calcite dendrite crystals growing on pool floor consisting densely laminated fabric. (C) Thin section photomicrographs of calcite crystals organised into a fan-shaped dendritic morphology. Crossed polarized light. (D) Layers of laminated boundstone locally disrupted by isolate sub-spherical to lenticular pores; the majority of them are trapped between dense laminated layers and thin undulated sheets of micrite. (E) Alternation of banded porous laminated boundstone composed of micrite and microsparite and dense laminated boundstone composed of dense micrite. (F) Laminated boundstone with drib lobe-like laminated structures. (G) Thin section photomicrographs of alternating layers of micrite (dark) and microsparite (white) laminae. Note that lamination may be observed within the laminae. (H) Raft boundstone/rudstone with thin film structures. Note the intra-raft porosity. (I) Coated bubble boundstone with hollow carbonate-coated microstructures. (J) Thin section photomicrograph of lithified gas bubbles with honeycomb-like porous structure. (K) Lithified gas bubbles showing linear distribution pattern. (L) Isolated lithified gas bubble with inner wall lined by scalenohedral sparite cement.

slight rain, degassing or wind-induced agitation of the water surface can cause the raft breakage and collapse at the bottom of the pool (Croci et al., 2015; Gandin & Capezzuoli, 2014).

#### 4.4. Coated gas bubble boundstone (FC4)

##### 4.4.1. Description

Coated gas bubble boundstone is represented by hollow carbonate-coated microstructures that are diverse in shape (Figure 4(I)–(L)). The encased space is lined by thin beige to white calcite. Accumulated and lithified gas-filled bubbles can develop layers (3 cm thick), honeycomb-like porous structure (Figure 4(J)), that grow and hold a spherical shape while calcite crystallised on their surfaces. The distribution of these lithified bubbles can show a linear pattern (Figure 4(K)) controlled by the planar shape of their substrate. Lithification, readily concomitant with the bubble development, is represented by micrite thin layers ranging in thickness from 10 to 30  $\mu\text{m}$ . The inner wall of the lithified gas bubble is lined by scalenohedral sparite cement (Figure 4(L)).

##### 4.4.2. Interpretation

Coated bubble boundstone facies are reported to occur on the planar surfaces of ponds and pools of terraced slopes (Chafetz & Folk, 1984; Croci et al., 2015; Guo & Riding, 1998). Their development is ascribed principally to rapid precipitation from slowly flowing laminated waters (Jones & Renaut, 2010). Many carbonate-lithified gas bubbles are described in the travertine depositing systems around the world including Ichi River Japan (Kitano, 1963), Rapolano Terme, Italy (Chafetz & Folk, 1984; Folk & Chafetz, 1983), eastern Idaho, USA (Chafetz & Meredith, 1983; Chafetz et al., 1991), Yellowstone National Park, Wyoming, USA (Pursell, 1985) and southern Germany (Koban & Schweigert, 1993).

#### 4.5. Reed boundstone/rudstone/grainstone (FC5)

##### 4.5.1. Description

They include stem and branch moulds and leaf imprints (Figure 5(A)). The main part of stem moulds preserves their original upright position with heavy carbonate encrustation composed of alternating bands of porous and dense micrite with variable band numbers and thicknesses ranging from 6 to 8 bands and from 2- to 3-mm thick, respectively. Moulds of reed stem are also abundant and can be either horizontally crowded (layers of 50 cm) and encrusted.

##### 4.5.2. Interpretation

Plants and prokaryotes are always present in the majority of spring systems where water is maintained with constant supply, composition and temperatures that do not

exceed their degree of tolerance to survive (Jones & Renaut, 2010). According to Jones and Renaut (2010), plant moulds diversity, density and distribution can indicate changes in the temperature of spring waters (cooling gradient) towards plant-tolerated temperatures as they flow downstream in the relatively distal sites and are almost absent in the vicinity of the ridge fissures or spring vents.

#### 4.6. Coated grains (FC6)

##### 4.6.1. Description

They are represented by grains with a nucleus coated by cortical laminae (Figure 5(B) and (C)). Their density varies from scattered to densely packed and their size ranges from 0.5 to 3 cm in diameter. Cut pisoids (Figure 5(C)) show closely packed concentric to sub-concentric cortical laminae consisting of lamina couplets of dense dark and porous light micrite ranging in number from 10 to 20 dark laminae and 15 to 30 light laminae. Some of the laminae are more visible than others due to their low content of dark pigments (Fe and Mn oxides).

##### 4.6.2. Interpretation

Pisoids can develop in many different types of spring systems (Andrews & Brasier, 2005; Chafetz et al., 1991; Ford & Pedley, 1996; Guo & Riding, 1998, 1999; Pentecost, 2005) and they have been ascribed to inorganic processes associated with bacterial mediation in pools that periodically agitate (Jones & Renaut, 2008). Some variations of pisoid shape are interpreted to be induced by the shape of their nucleus (Pentecost, 2005).

#### 4.7. Aquatic insect larval tube boundstone (FC7)

##### 4.7.1. Description

These particular facies consist of calcified cylindrical insect larval tubes giving the rock an appearance of roughly porous fabrics (Figure 5(D)). Tubes are arranged in layers (up to 5 cm thick) with the individual tubes oriented normal to the bedding, roughly parallel to each other and slightly narrower to the base of the bed. Tubes are 5–10-mm long and 3 mm in diameter (Figure 5(E)). The upper cephalic ends of the tubes are open with remarkable funnel-like openings. Inner tube walls are lined with 0.1–0.5-mm-thick beige to white dense micrite rings encased in a more thick and porous white micrite envelop that constitutes the main tube framework.

##### 4.7.2. Interpretation

These facies are interpreted as calcified insect larval retreats (Carthew, Taylor, & Drysdale, 2002; Drysdale, 1998, 1999; Drysdale et al., 2003). Based on the overall dimensions of the tubes, their arrangement and the texture of the inner tube micrite ring are interpreted as

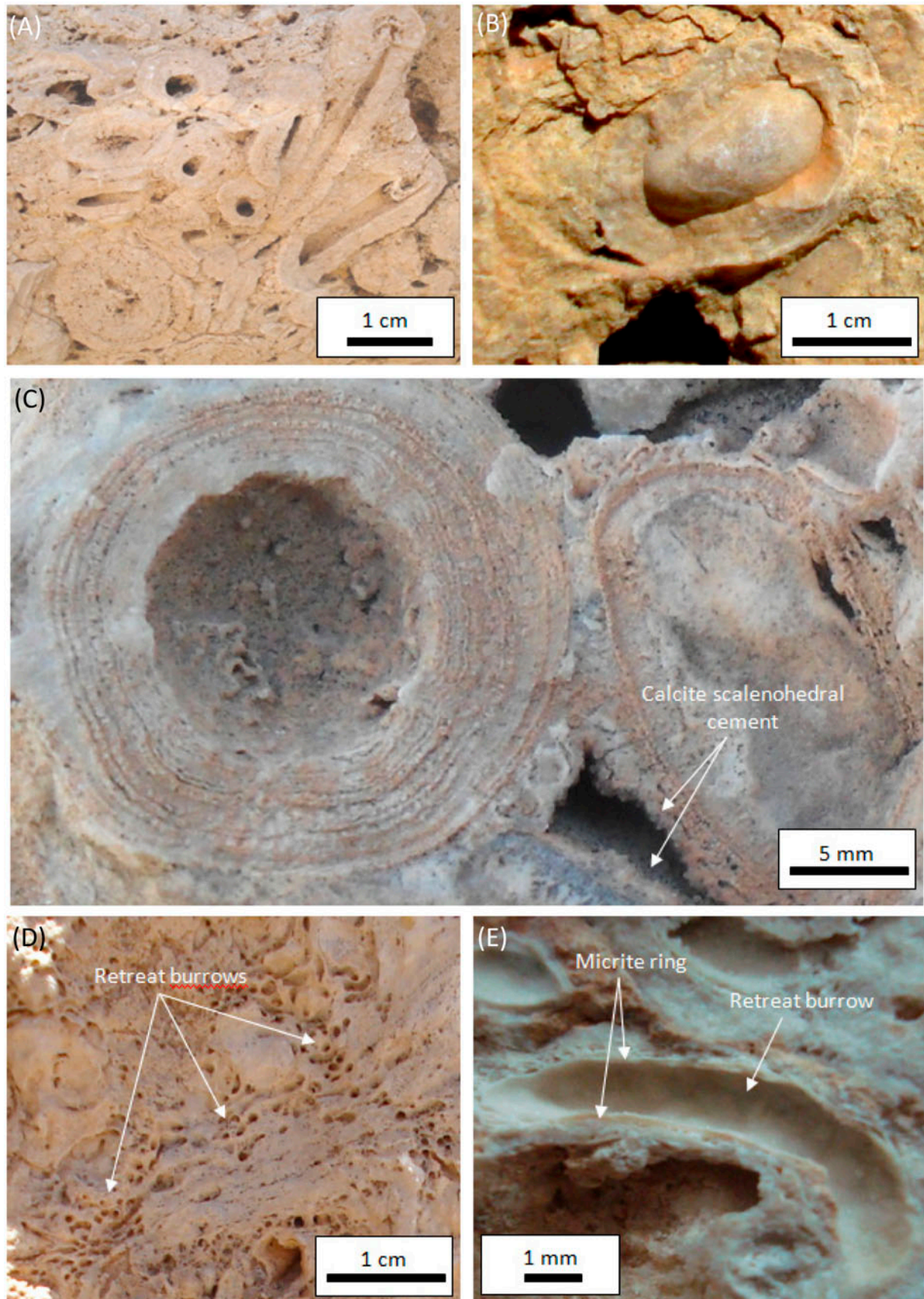


Figure 5. (A) Reed boundstone including stem and branch moulds; some of them are in their original upright position with heavy carbonate encrustation. (B) and (C) Coated grain (pisoid) showing closely packed concentric to sub-concentric cortical laminae consisting of lamina couplets of dense dark and porous light micrite ranging in number from 10 to 20 dark laminae and 15 to 30 light laminae. (D) Aquatic insect larval tube boundstone consisting of calcified cylindrical insect larval tubes arranged in layers and oriented normal to bedding. (E) Details of one pyralid larval tube. Tube inner wall is lined with 0.1–0.5-mm-thick white dense micrite ring encased in a more thickly porous white micrite envelop.

Pyralidae (order: Lepidoptera) larval cases (Carthew et al., 2002; Drysdale, 1998). Pyralid larval cases are constructed by silken structures, in the form of tube-like (burrow) cases (Carthew et al., 2002). However, this is not only the silken structure in which pyralid insects construct their larval cases but also the marquee shelters (rectangular structures) are as widespread as the tube-like cases depending on the ecological behaviour of the insect. According to Carthew et al. (2002), these burrows may indicate a preferential hydraulic environment within the travertine depositional system represented by gently flowing water over the travertine masses where open ends of the tubes face the current direction of flowing waters. These cases are constructed using the salivary silk secretions of pyralid insects to bind the detritus, algae and small animal debris to form the tube framework (Benke, Van Arsdall, Gillespie, & Parrish, 1984).

#### 4.8. Disorganised matrix-supported conglomerates (FT1)

##### 4.8.1. Description

These facies consist of matrix-supported conglomerates with sub-angular to sub-rounded and poorly sorted cobble-boulder clasts (Figure 6(A)) (clast size ranging

from few centimetres to 1 m) with disorganised fabric. Crude imbrications are common as well as major channellised bases and possibly large flute marks or sharp truncations. The conglomerate layers, with thickness ranging from 0.5 to 2 m and decreasing towards the S–SE direction, stand out as crudely bedded terraces. The total number of these conglomeratic bars within the outcrop succession varies from 15 to 20 bars representing normal and inverse grading. The fabrics of the coarser clasts are disorganised and rarely graded. The lithological composition of the clasts consists of <70% limonite-stained boulders. Elongate boulders are also common and aligned parallel to bedding and concentrated just above the basal portion of the beds. The matrix shows two main components: (1) a detrital matrix consisting of terrigenous silty sand and (2) locally massive micrite and microsparite (Figure 6(B)).

##### 4.8.2. Interpretation

These conglomerates of poorly sorted, muddy matrix-supported gravel and chaotic fabrics are interpreted as a deposition by cohesive clast-rich debris flow (Blair, 1987; Miall, 1996). The remobilisation of debris flow by water action is evidenced by the presence of

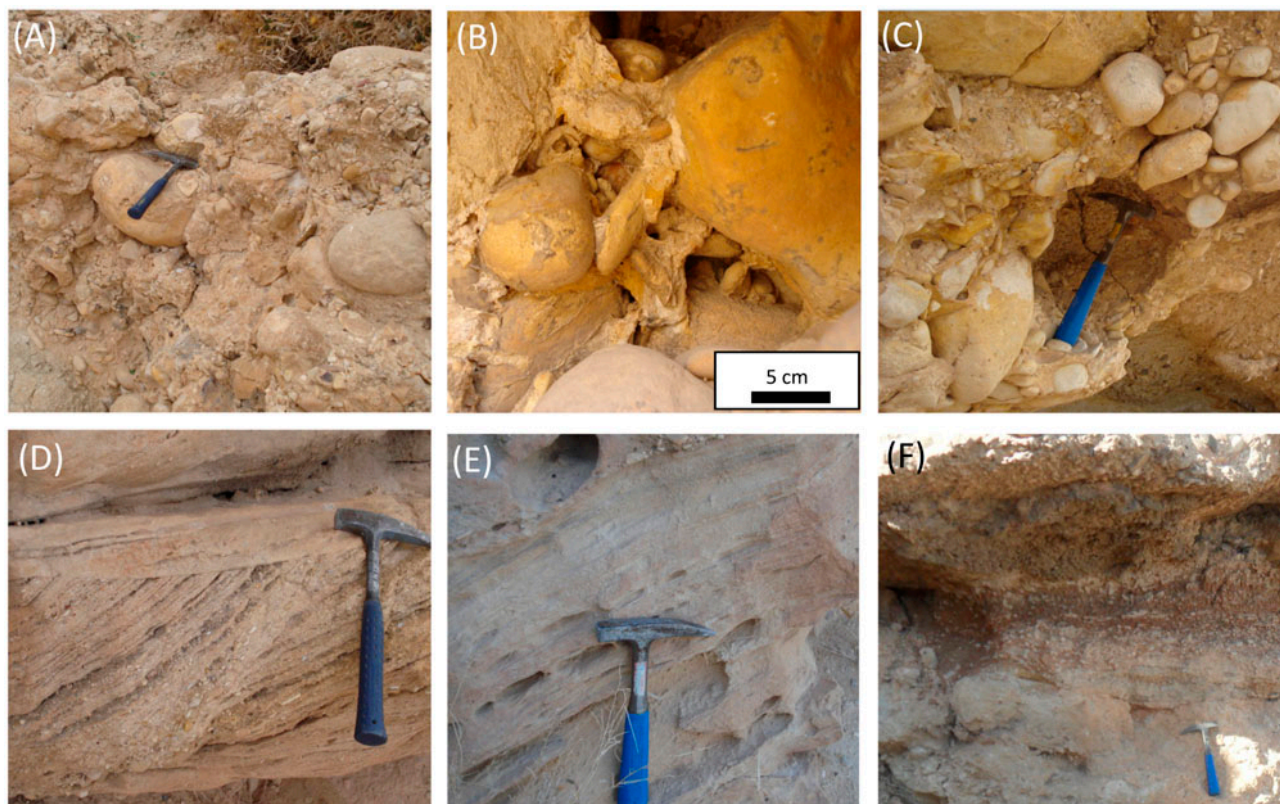


Figure 6. Alluvial fan lithofacies. (A) Disorganised matrix-supported conglomerates (FT1) composed of matrix-supported sub-angular to sub-rounded and poorly sorted cobble-boulder clasts. (B) Conglomerates with structureless micrite and microsparite matrix. (C) Disorganised matrix- to clast-supported conglomerates (FT2). (D) Stratified sandstones (FTS1). Note that set and coset thicknesses of cross-strata average between 20 and 35 cm and 1 and 1.5 m, respectively, with low-angle cross-strata dipping from 15 to 25°. (E) Massive sandstones (FTS2). (F) Massive mudstones (FT3) with calcareous pedogenic nodules and reddish-brown claystones.

crude-stratified gravel. The development of an alluvial fan body by debris flow deposition is documented in ancient and modern examples (e.g. Bull, 1977). The debris flow is defined by Blair & McPherson, 1994 as a type of sediment-gravity flow composed of a mixture of gravel, sand, clay and a small amount of entrained water driven downslope by the force of gravity. The origin of the intergranular filling by micrite and/or microsparite is probably ascribed to deposition under subaquatic low energy conditions in alluvial plain shallow ponds (Croci et al., 2015).

#### 4.9. Disorganised matrix- to clast-supported conglomerates (FT2)

##### 4.9.1. Description

These facies consist of disorganised, poorly sorted, ungraded and matrix- to clast-supported pebble, cobble to boulder clasts (Figure 6(C)). The clast size varies from few centimetres to 80 cm with sub-rounded to rounded shapes. The large boulders lie along the basal contacts and are spaced several metres away. Bedding thickness averages between 20 and 60 cm. Beds have irregular basal contacts with lens-shaped geometry with non-stratified and chaotic fabric. The matrix is composed of a mixture of the same matrix components seen in FT1 plus coarse sand-granule matrix. Facies FT2 interfingers and intercalates vertically and laterally with FT1 with remarkable abundance of cobble-sized clasts within a polymodal clast distribution. Locally, they can show heavily encrusted fractures with white calcite veins.

##### 4.9.2. Interpretation

The sedimentary rock attributes of FT2 suggest a rapid deposition pattern induced by hyperconcentrated flood flow triggered by catastrophic flood events and/or heavy rainfall and cloud bursts (Lavigne & Suwa, 2004). According to (Nichols, 2005), hyperconcentrated flow has been recognised in instances where the catchment area was relatively small or where the hinterland bedrock was dominated by mudstones and evaporites. The fractures showing calcite encrustation are interpreted as conduits for carbonate-enriched fluids.

#### 4.10. Stratified sandstones (FTS1)

##### 4.10.1. Description

These facies FS1 are present locally at the base of the central logged section (Log WT3) beneath the disorganised matrix- to clast-supported conglomerates FT2 and consist of medium- to coarse-grained gray sandstones with clearly visible normally graded trough cross-stratifications (Figure 6(D)). Set and coset thicknesses of cross-strata average between 20 and 35 cm and 1 and 1.5 m, respectively, with low-angle cross-strata dipping ranging from 15° to 25°. After removing the effects of dipping

and tilting related to faulting, these cross-stratifications indicate a south to south-east paleocurrent direction. Relatively large-scale cross stratifications with 50-cm-high set are also identified with tangential, concave-up cross-strata. FTS1 passes upward and laterally into more massive and/or pink-coloured planar and laminated sandstones. Horizontal and thinly laminated beige-coloured fine-grained sandstone layers are separated by only millimetre-thick marls partings that weather out leaving behind them a fabric-oriented porosity.

##### 4.10.2. Interpretation

Cross-stratifications are engendered by the downward migration of current ripples suggesting a relatively rapid deposition under waning stage of alluvial channel or by some other low-magnitude flow (Blair & McPherson, 1994; Miall, 1996).

#### 4.11. Massive sandstones (FTS2)

##### 4.11.1. Description

These facies consist of fine to very fine-grained moderately consolidated massive sandstones (Figure 6(E)). The beds are laterally discontinuous and range in thickness between 50 cm and 1 m and are interbedded with the disorganised matrix- to clast-supported conglomerates FT2. When they are overlain by FT2 and/or FT1, the transition is made through major channelled bases and possibly large flute casts and crude imbrications. Locally, these facies can contain prehistoric flint stone tools composed of lithic flakes, hand axes, burins and scrapers of late Acheulian age (Collignon, 1887; Gobert, 1952; Vaufrey, 1933) which are commonly dispersed with no preferential graded and/or oriented distribution.

##### 4.11.2. Interpretation

This facies is interpreted as being deposited by rapid sedimentation through gravity-flow in shallow water ponds. Locally, they can represent the conglomeratic bar surface deposits of an alluvial floodplain (Miall, 1996).

#### 4.12. Massive mudstones (FT3)

##### 4.12.1. Description

These facies consist of green, reddish brown to yellow-coloured massive (to slightly laminated) and thickly bedded siltstones and claystones (Figure 6(F)) that occur throughout lower portions of entire logged sections. They show irregular contacts with overlying beds. Locally, root cast and incipient pedogenic features (calcareous concretions with size ranging from 1 to 4 cm in diameter) can be identified randomly distributed with the reddish brown (Dry colour: 5YR 4/4 – reddish brown) claystones.

#### 4.12.2. Interpretation

The fine-grained nature and the uniform texture of the siltstones and claystones are interpreted as over bank deposits (Blair & McPherson, 1994; Miall, 1996). The calcareous concretions indicate pedogenic activity and paleosol stage in the fan system (Alçiçek & Alçiçek, 2014; Croci et al., 2015; Miall, 1996).

### 5. Facies associations and reconstruction of depositional environments

#### 5.1. Terraced slope travertine lithofacies association

Terraced slope travertine lithofacies association is located in the lower portion of the travertine–terrigeneous succession and recorded in the stratigraphic Log WT1 of the western compartment of Jebel El Mida. It comprises the facies group FC1–FC6 and shows clear massive and bedded structures with white greyish colour and weakly porous fabrics. These deposits are considered as the first generation of travertine (Figure 7). The travertine bedding plane surfaces show undulating structures with many protuberances and corrugations when restored to their original horizontal position by removing the tectonic tilting. They reveal much about their lateral continuity and the flowing direction of spring waters and even the distribution patterns of the overlying conglomerates. Figure 7(A)–(C) shows the general morphology of the travertine with the conglomerates, consisting of discernible pools of terraced slope system with rims and walls oriented to the south-east. Coarser boulders, cobbles and pebbles occupy the deepest and sheltered depressions of the terraced slope system in form of entrapments. The paleocurrent reading of fining upward detrital elements shows a south to south-east transport direction of the alluvial fan drainage.

#### 5.2. Fissure ridge travertine lithofacies association

The fissure ridge travertine lithofacies association is recorded in the stratigraphic logs of the eastern compartment of Jebel El Mida (Logs ET1, ET2 ET3) and represented by the lateral and vertical transition of FC1–FC7. The uppermost denudated surfaces of the ridge (Figure 8(A)) can reveal small-scale ephemeral pools with rims (Figure 8(B)), with centimetres deep and less than a metre extend. Travertine discharge apron indicates the outlets of small springs within the fissure. The spring thermal pools show densely cemented rocks composed of shrubs of cyanobacterial growth (FC1). In the thin sections, these rocks reveal a laminated structure (FC2). Many en-echelon and bifurcated fissures run sub-parallel along the ridge crest (Figure 8(C) and (D)). The aperture varies from 5 to 15 cm with inner fissure walls coated with 2–6-cm-thick banded travertine. The last generation of this banded travertine shows laminated structures. The eastern margins of the ridge (Figure 8(E) and (F)) reveal either lenses of travertine encased in former channelled

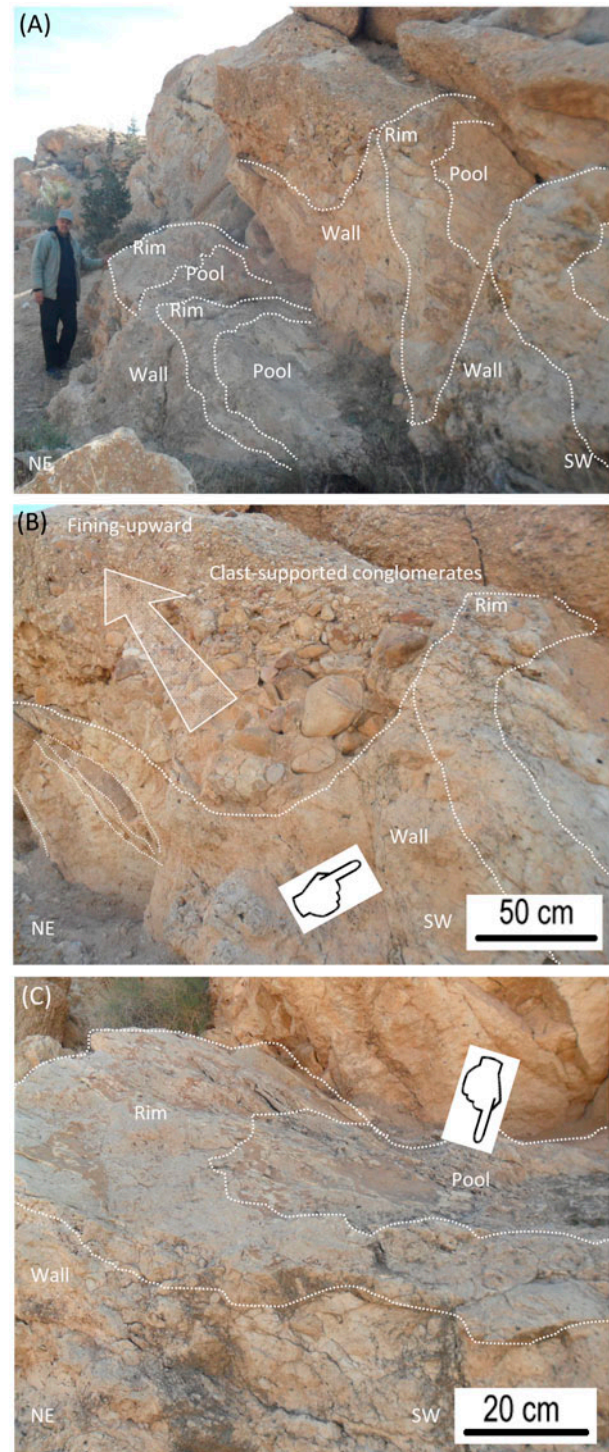


Figure 7. Terraced slope travertine lithofacies association. (A) Discernible pools of terraced slope system with rims and walls oriented to the south-east and overlain by discharged coarse terrigenous materials. (B) and (C) Details of (A) showing the architecture of the travertine and the alluvial deposits.

streams and alluvial plain or isolated or relatively rounded travertine slabs encased in fine-grained sandstone facies (FTS1–FTS2). Along the lower elevated reaches, the travertine ridge body can extend southwards and downslope (Figure 8(G)) where it is encased and



Figure 8. Fissure ridge travertine lithofacies association. (A) Uppermost denudated surfaces of the ridge. (B) Small-scale ephemeral pools with rims. (C) En-echelon and bifurcated parasitic fissure. (D) Crestal fissure showing banded travertines. (E) Eastern margins of the ridge showing lenses of travertines encased in former alluvial plain channelised streams. (F) Isolated rounded travertine slabs encased in pebbly to fine-grained sandstone facies. (G) Southward downslope margins of the ridge encased and overlain by coarse matrix- to clast-supported alluvial conglomerates. (H) North-eastern margins of the ridge show accumulations of porous travertine around parasitic fissures developed on matrix-supported gravels.



overlain by coarse matrix- to clast-supported alluvial conglomerates (FT1 and FT2). The north-eastern parts of the ridge show accumulations of porous travertine around parasitic fissures which were developed on matrix-supported gravels (Figure 8(H)).

### 5.3. Alluvial fan lithofacies association

The visual alluvial fan deposits recorded in the six stratigraphic logs are distributed in paleostreams and interfingering in the eastern and western parts of Jebel Mida with travertine masses (Figure 9(A)). The alluvial fan lithofacies association is consisted of conglomerates and sandstones lithofacies (FT1, FT2, FTS1 FTS2 and FT3) ranging in thickness from 80 to 120 m. These deposits are arranged in fining upward sequences indicating waning flow conditions. The coarser fanglomerates with sandstone facies are developed as debris flows and streamflood deposits (Figure 9(B) and (C)). In Jebel El Mida, these alluvial deposits interfinger with and overlain by travertine deposits (Figure 9(D)).

### 5.4. Reconstruction of depositional events

Based on the vertical and lateral stratigraphic architecture of the travertine and terrigenous successions studied

herein, two depositional phases can be distinguished for the travertine interfingering with alluvial deposits. A possible paleoenvironmental reconstruction of the different depositional phases is summarised in Figure 10.

#### 5.4.1. Phase I

This phase (Figure 10(A)) is marked by the deposition of the western travertine at the base of the succession in the form of terraced slope mounds with a south to south-east dipping and thinning. This orientation indicates the location of the hydrothermal springs and the paleoflow direction in the immediate vicinity of the Gafsa Fault. The deposition of the travertine is assured by fault-related hydrothermal springs suggesting a tectonic activity of the Gafsa Fault during early Pleistocene time (Henchiri, 2014a). This tectonic activity has provided conjugated faults for the travertine deposition and also the relief accommodating the alluvial fan deposition. The earlier NW–SE-trending dextral strike-slip faults with normal components linked to the Gafsa Fault have resulted in subsidence to create the depression where the alluvial fan deposited. The coarse clastic alluvial fan body is surrounded by fine-grained alluvial plain deposits with a limited number of individual alluvial fan apexes. Such spatial distribution of the alluvial fan facies

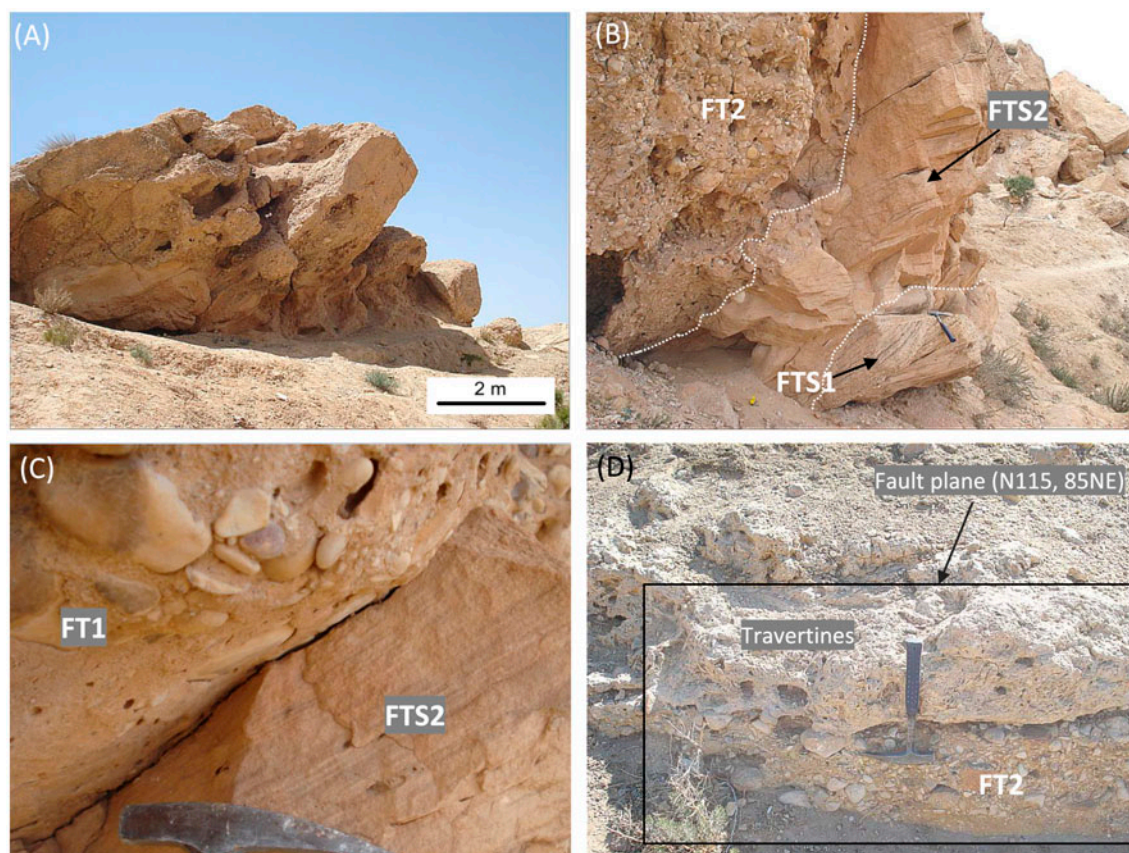


Figure 9. Alluvial fan lithofacies association. (A) Uplifted and extensively eroded fanglomerates and sandstones lithofacies. (B) and (C) Coarser fanglomerates with sandstone facies are developed as debris flows and streamflood deposits. (D) Alluvial deposits interfingering with travertines.

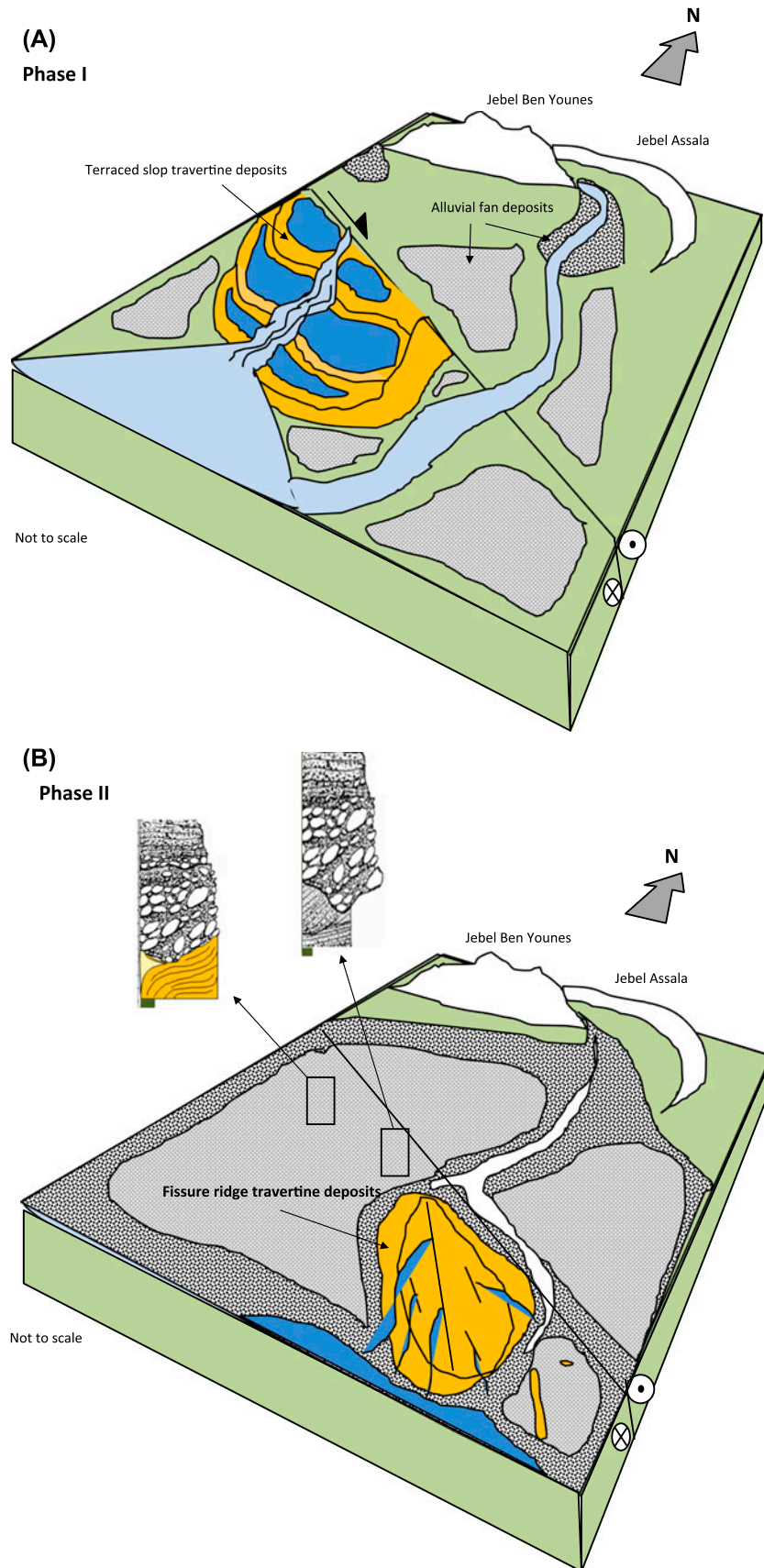


Figure 10. A possible paleoenvironmental reconstruction of the different depositional phases. See text for details. (A) Phase I, the development of terraced slope depositional system triggered by inherited extensional normal faults associated with the GF. (B) Phase II, characterised by the onset of alluvial discharge and the change of the tectonic regime from transensional to transpressional fissure ridge travertine depositional system.

associations has been interpreted as the result of a drainage network that was expanding in the catchment area (hinterland drainage network) and localised between the structures of Jebel Ben Younes and Jebel El Assala. Overall, the alluvial fan sediments of Jebel El Mida record the history of sediment dispersal and deposition in sedimentary basin adjacent to a mountain belt. These alluvial sediments were formed by periodic flash-flood sedimentation in arid to semi-arid settings.

5.4.2. Phase II

This phase (Figure 10(B)) is characterised by the filling up of the former drainage network and the onset of clay-rich sandy alluvial/colluvial plain deposits. It is

concomitant with a second travertine deposition phase that occurred through intermittently synsedimentary reactivated faults linked to the GF forming the fissure ridge depositing system. Co-existence of the travertine and the alluvial plain deposits during early stages of phase II is well materialised by the interfingering between both lithofacies in many places of the depositing system such as the travertine filling up of channelised streams and the sand-encased travertine blocks. The rapid growth of the travertine ridges has exceeded the slow alluvial plain development that resulted in the preservation of the ridges from flash flooding and coarse debris flow sedimentation which overlain only the low-elevated travertine masses in relatively distal sites. This depositional phase is associated with an upper Acheulean stone tools

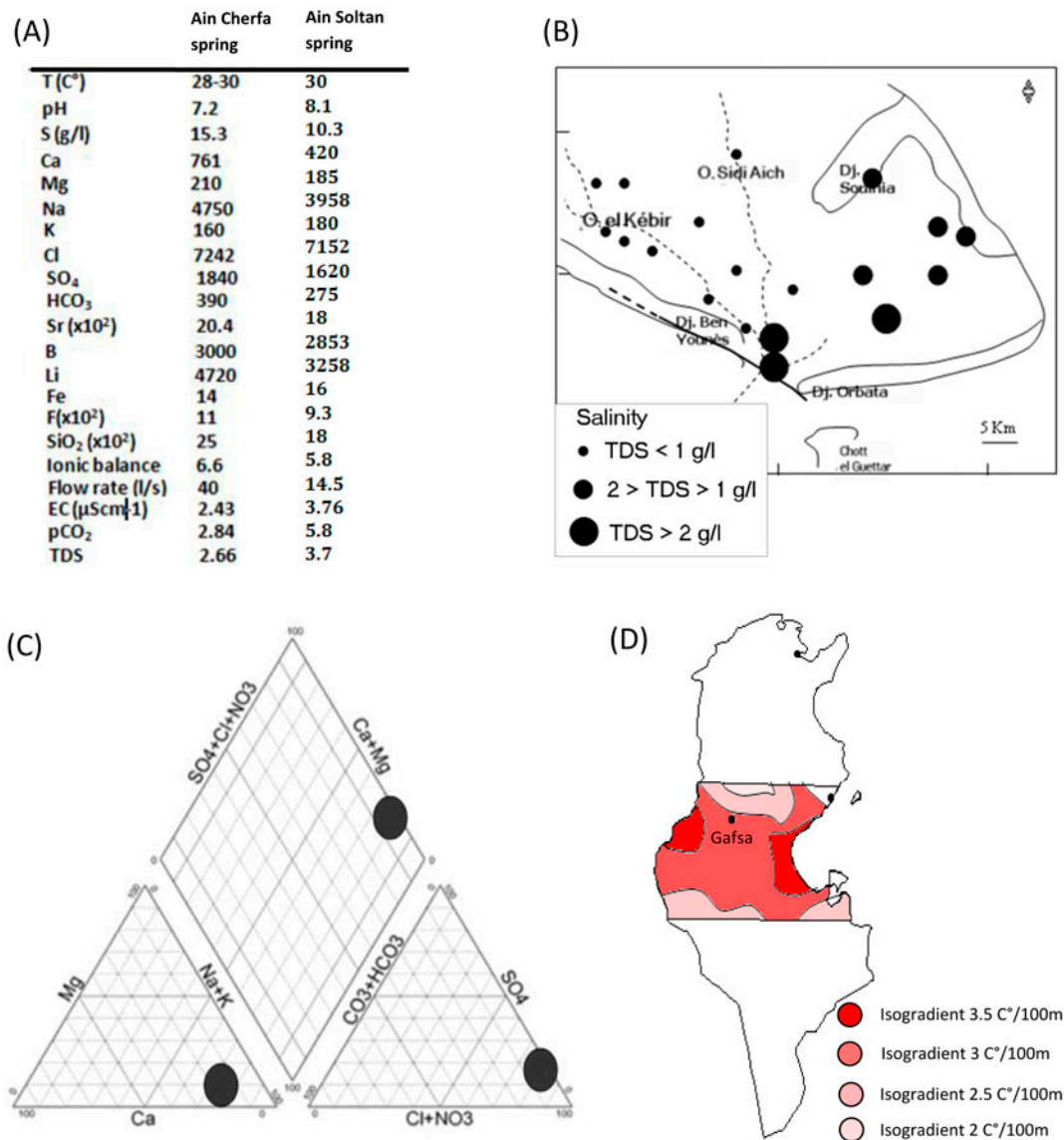


Figure 11. (A) Geochemical composition of Ain Cherfa (near Jebel Ben Younes) and Ain Soltan (near Jebel Orbata) (data provided by CRDA Gafsa). (B) Distribution pattern of the salinity in the groundwaters near Gafsa. (C) Piper plot of the water samples from Ain Cherfa and Ain Soltan. (D) Geothermal gradient map of Gafsa (modified from Ben Dhia, 1990).

industry which was ascribed to early human (i.e. *Homo habilis*) by Collignon (1887), Vaufrey (1933) and Gobert (1952).

## 6. Chemical composition of the Gafsa Fault active springs

Hydrochemical parameters of water from some active springs along the Gafsa Fault near Jebel El Mida, including water temperature, pH, EC,  $p\text{CO}_2$ , TDS, major and minor ions, were provided by the CRDA Gafsa (Commissariat Régionale au Développement Agricole) (Figure 11). The selected samples (from Ain Cherfa near Ben Younes and Ain Soltan near Orbata, see Figure 1) are characterised by a temperature averaging 30 °C and groundwater pH values ranging between 6.76 and 8.1 (Figure 11(A)). The  $p\text{CO}_2$  ranges between  $1.32 \times 10^{-2}$  and  $5.38 \times 10^{-2}$  atm compared with the precipitation  $p\text{CO}_2$  of  $10^{-3.5}$  atm. The EC varies between 0.72 and 9.15  $\mu\text{S cm}^{-1}$ . Higher values have been found near the GF (hydraulic sill). The total dissolved solids (TDS) range from 0.5 to 15  $\text{g l}^{-1}$  (Figure 11(B)). The springs have very similar chemical composition (Figure 11(C)) which are characterised by a very high amount of  $\text{SO}_4^{2-}$ ,  $\text{Ca}^{2+}$  and  $\text{Mg}^{2+}$  coupled with a relatively high amount of  $\text{HCO}_3^- + \text{CO}_3^{2-}$ . These springs have high contents of Sr, which, collectively sulphates and bicarbonate, indicate an interaction of fluids with a carbonate and evaporite succession.

## 7. Discussion

Hydrothermal activity along GF has been attributed to the result of the interaction between heat source, circulating fluids and permeability pathways (Saïd et al., 2011). The circulating hydrothermal fluids are of meteoric origin and were contaminated by a continuous water–rock interaction (Edmunds et al., 2003). The region of Gafsa is characterised by geothermal gradients ranging from 25 to 35° per km (Figure 11(D)) (Ben Dhia, 1990). This anomaly is mainly controlled by the NW–SE-trending strike-slip GF suggesting a strict control of such a structure in fluid flow circulation in a convective geothermal system. Deep water percolation and flow at depths of 1000 m or more (Lower Cretaceous ‘Sidi Aïch Formation’ 1000 m deep and the Upper Cretaceous ‘Zebbag Formation’  $\approx$  340 m deep) increase the temperature of water by a variety of processes through which carbonate dissolution is enhanced by increase of water temperatures resulting from a deep-seated geothermal source since the study area is characterised by a relatively high local geothermal gradient and active tectonics (Ben Dhia, 1990). On migration to the surface, these  $\text{CO}_2$  gas-enriched solutions undergo rapid cooling and  $\text{CO}_2$  loss, which shift the equilibrium position of calcium-bicarbonate groundwater to the travertine formation. Permeability pathways for these  $\text{CO}_2$ -enriched waters result from fault movement that fractures the rocks and, in turn,

increase the overall permeability and thus generate new fluid paths to the surface (Caine, Evans, & Forster, 1996). Highly fractured rocks contribute sufficiently in the penetration of meteoric waters to deeper levels and mixing with other fluids of deep origin with the possible production of highly bicarbonate-enriched waters through reaction with carbonate rocks.

The travertine formation during lower to middle Pleistocene at Jebel El Mida implies the existence of paleohydroclimatic conditions characterised by abundant effective rainfall in the recharge zone. The second parameters are a dense vegetation cover, organic-rich soils that permit the percolation of acidic (aggressive) waters, the dissolution of the aquifer carbonate rocks and bicarbonate-enriched waters. It is noteworthy that the climatic, hydraulic and pedologic conditions that prevail during the travertine precipitation can be largely different from those prevailing during groundwater recharge. A gap between the two events is likely due to the speed of the water flow in the aquifer, which can only be estimated very roughly in ancient times and may be in some cases over last thousands of years (Marsily, 1981; Roche & Thiery, 1984). Radiocarbon dates of peaty material associated with continental carbonates (tufa) from Jebel Ben Younes (Henchiri, 2014b) to the west of Jebel El Mida reveal more younger deposits in the western parts of the Gafsa Fault. This may represent the continuity of the carbonate deposition from the springs that emerge from the fault after the uplift of the structure of Jebel El Mida and eventually dissect its travertine depositing system.

The U/Th radiometric dating of water and carbonates of land snail shells from Oued Akarit in Gabès region (95 km to the SE of Gafsa) shows the existence of four major rain phases and flooding events during middle to late Pleistocene (180–200, 130–150, 95–100 and 30 Ka BP) (Causse et al., 2003). In the Maknassy basin (55 km to the NE of Gafsa), the analysis of the carbonates of land snail shells dating from middle to late Pleistocene confirms the existence of several humid phases (Ouda, Zouari, Ben Ouedzou, Chkir, & Causse, 1993) more or less identical with those recorded in Oued Akarit. In the region of Chott El Gharsa (50 km to the SW of Gafsa), Swezey (1997) and Blum et al. (1998) have shown the existence of four lacustrine cycles (terraces) preserved within the series of incised valleys. Thermoluminescence dating of these terraces (Blum et al., 1998) gave ages of 111 Ka BP for the first, 108 ka BP for the second, 85 Ka BP for the third and 21 Ka BP for sub-recent terraces. These lacustrine cycles were characterised by the stabilisation of sand dunes of Chott El Gharsa by vegetation and raised groundwater levels. Correlatively in the region of Gafsa, which occupies the central location between these three neighbouring regions, it was inferred that there were same paleoclimatic events which contributed to sufficient recharge of the groundwater, the travertine development and the occurrence of alluvial deposition.

## 8. Conclusion

The morphotectonic and sedimentological study of a mixed travertine–alluvium succession at Jebel El Mida in southern Tunisia has led to the following conclusions:

- (1) The Quaternary stratigraphic record of Gafsa region shows at Jebel El Mida a mixed stratigraphic succession composed mainly of travertine and detrital terrigenous materials. Their distribution patterns and accumulation rates are function of tectonic and climatic variables.
- (2) The travertine deposition takes place in a wide strike-slip-faulted and uplifted early to middle Pleistocene alluvial fan. Seven travertine facies (FC1–FC7) gave rise to terraced and fissure ridge-type travertine lithofacies associations, respectively.
- (3) The depositional events of travertine comprise a terraced slope travertine composed of the facies group FC1–FC6 which shows clear massive and bedded structures with white greyish colour and weakly porous fabrics bounded to the north-east by grainy travertine. Their deposition was interpreted to be triggered by inherited extensional conjugated fault system from the Gafsa Fault. The second depositional event is characterised by the onset of fissure ridge travertine composed of the facies group of FC1–FC7. Both depositional systems are separated in time and space and as interfingering with alluvial fan channels and alluvial plain deposits.
- (4) The hydrothermal activity feeding development of travertine at Jebel El Mida is a result of the interaction between heat source, circulating fluids and permeability pathways. The heat source is originated from a relatively high local geothermal gradient and active tectonics. The circulating fluids come from deep (1000 m) Aptian carbonate-enriched groundwaters (Sidi Aich and Zebbag formations, respectively). The permeability pathways are provided by highly damaged rocks in the vicinity of the active strike-slip Gafsa Fault.
- (5) The paleoclimatic correlation with neighbouring localities reveals the existence of many humid episodes during early to middle Pleistocene. It has a possible contribution for sufficient recharge of the groundwater, the travertine development and the occurrence of alluvial deposition. This phenomenon has resulted in the stratigraphic record as the net sum of the tectonic activity, the rise and fall of the water table and associated climatic change.

## Acknowledgements

The authors would like to thank the staff of the CRDA Gafsa for providing hydrochemical data of the GF spring waters. We

are grateful to Dr. Russell Neil Drysdale from the University of Melbourne, Australia for confirming the insect larval origin of some travertine structures studied herein. Special thanks to M. Gharbi for help during field work and discussion. MCA thanks to the Outstanding Young Scientist Award given by Turkish Academy of Sciences (TUBA-GEBIP).

## Disclosure statement

No potential conflict of interest was reported by the authors.

## ORCID

Mohsen Henchiri  <http://orcid.org/0000-0002-1493-0343>

Andrea Brogi  <http://orcid.org/0000-0002-3386-3609>

Mehmet Cihat Alçiçek  <http://orcid.org/0000-0001-7689-7625>

## References

- Abdeljaouad, S. (1991). *Les doloc retes et les calcr tes du Pal oc ne-Eoc ne (Tunisie M ridionale)* (Th se) [Paleocene-Eocene dolocretes and calcretes of southern Tunisia, PhD Thesis], (242 pp). Tunisia: University de Tunis II.
- Alçiçek, H., & Alçiçek, M. C. (2014). Palustrine carbonates and pedogenic calcretes in the  al basin of SW Anatolia: Implication on the Plio-Pleistocene regional climatic pattern in the eastern Mediterranean. *Catena*, 112, 48–55.
- Altunel, E., & Hancock, P. L. (1993a). Active fissuring and faulting in Quaternary travertine at Pamukkale, western Turkey. *Zeitschrift f r Geomorphologie Supplement Series (Z. Geomorphol. Supp.)*, 94, 285–302.
- Altunel, E., & Hancock, P. L. (1993b). Morphology and structural setting of Quaternary travertines at Pamukkale, Turkey. *Geological Journal*, 28, 335–346.
- Andrews, J. E., & Brasier, A. T. (2005). Seasonal records of climatic change in annually laminated tufas: Short review and future prospects. *Journal of Quaternary Science*, 20, 411–421.
- Atabey, E. (2002). The formation of fissure ridge type laminated travertine-tufa deposits: Microscopical characteristics and diagenesis, Kır ehir central Anatolia. *Mineral Resource Exploration Bulletin*, 123–124, 59–65.
- Ben Ayed, N. (1986). *Evolution tectonique de l'avant pays de la cha ne alpine de Tunisie du d but du M sozoique   l'Actual* [Tectonic evolution of the Alpine chain of Tunisia from Early Mesozoic to the present] (PhD Dissertation), (328 p). Tunis.
- Ben Dhia, H. (1990). Application of chemical geothermometers to some Tunisian hot springs. *Geothermics*, 19, 15–23.
- Benke, A. C., Van Arsdall, T. C., Gillespie, D. M., & Parrish, F. K. (1984). Invertebrate productivity in a subtropical blackwater river: The importance of habitat and life history. *Ecological Monographs*, 54, 25–63.
- Blair, T. C. (1987). Tectonic and hydrologic controls on cyclic alluvial fan, fluvial, and lacustrine rift-basin sedimentation, Jurassic-lowermost Cretaceous Todos Santos Formation, Chiapas, Mexico. *Journal of Sedimentary Research*, 57, 845–862.
- Blair, T. C., & McPherson, J. G. (1994). Recent Debris flow processes and resultant forms and facies of the Dolomite alluvial fan, Owen Valley, California. *Journal of Sedimentary Research*, 68, 800–818.
- Blum, M., Kocurek, G., Swezey, C., Deynoux, M., Lancaster, N., Price, D., & Pion, J. C. (1998). Quaternary wadi, lacustrine, Aeolian depositional cycles and sequences, Chott Rharha basin, southern Tunisia. In A. Alsharhan, K. Glennie, G. Whittle, & C. Kendall (Eds.), *Quaternary deserts and climatic changes* (pp. 539–552). Rotterdam: A.A. Balkema.

- Boukadi, N. (1994). *Structuration de l'Atlas de Tunisie : Signification géométrique et cinématique des noeuds et des zones d'interférences structurales au contact de grands couloirs tectoniques* [Geometric and kinematic significance of knots and interference zones in the contact of the major tectonic corridors] (PhD Dissertation), (155 p). Tunis.
- Brogi, A., & Capezzuoli, E. (2009). Travertine deposition and faulting: The fault-related travertine fissure-ridge at Terme S. Giovanni, Rapolano Terme (Italy). *International Journal of Earth Sciences*, 98, 931–947.
- Brogi, A., Capezzuoli, E., Aqué, R., Branca, M., & Voltaggio, M. (2010). Studying travertines for neotectonics investigations: Middle-Late Pleistocene syn- tectonic travertine deposition at Serre di Rapolano (Northern Apennines, Italy). *International Journal of Earth Sciences*, 99, 1383–1398.
- Brogi, A., Alçiçek, M. C., Yalçiner, C. C., Capezzuoli, E., Liotta, D., Meccheri, M., ... Shen, C. C. (2016). Hydrothermal fluids circulation and travertine deposition in an active tectonic setting: Insights from the Kamara geothermal area (western Anatolia, Turkey). *Tectonophysics*, 680, 211–232. doi:10.1016/j.tecto.2016.05.003
- Brogi, A., Capezzuoli, E., Alçiçek, M. C., & Gandin, A. (2014). Evolution of a fault-controlled fissure-ridge type travertine deposit in the western Anatolia extensional province: The Çukurbağ fissure-ridge (Pamukkale, Turkey). *Journal of the Geological Society, London*, 171, 425–441.
- Bull, W. B. (1977). The alluvial fan environment. *Progress in Physical Geography*, 1, 222–270.
- Caine, J. S., Evans, I. P., & Forster, C. B. (1996). Fault zone architecture and permeability structure. *Geology*, 24, 1025–1028.
- Capezzuoli, E., Gandin, A., Brogi, A., Ruggieri, G., Alçiçek, M. C., Liotta, D., ... Baykara, O. (2016). Onyx-like calcite veins: A challenging deposit for tracing the evolution of a sedimentary basin. *Quaternary International*, (submitted).
- Carthew, K. D., Taylor, M. P., & Drysdale, R. N. (2002). Aquatic insect larval constructions in tropical freshwater limestone deposits (tufa): Preservation of depositional environments. *Applied Entomology*, 31, 35–41.
- Castany, G. (1982). Bassin sédimentaire du Sahara septentrional (Algérie-Tunisie) – Aquifères du Continental intercalaire et du Complexe Terminal [Sedimentary basins of Northern Sahara (Algeria – Tunisia) – the aquifers of the Continental intercalaire and the Complexe Terminal]. *Bulletin BRGM*, 3, 127–147.
- Causse, C., Ghaleb, B., Chkir, N., Zouari, K., Ben Oueddou, H., & Mamou, A. (2003). Humidity changes in southern Tunisia during the Late Pleistocene inferred from U-Th dating of mollusc shells. *Applied Geochemistry*, 11, 1691–1703.
- Chafetz, H. S., & Guidry, S. A. (1999). Bacterial shrubs, crystal shrubs, and ray-crystal shrubs: Bacterial vs. abiotic precipitation. *Sedimentary Geology*, 126, 57–74.
- Chafetz, H. S., & Meredith, J. S. (1983). Recent travertine pisoliths (pisoids) from southeastern Idaho, U.S.A. In T. M. Peryt (Ed.), *Coated Grains* (pp. 450–455). New York, NY: Springer-Verlag.
- Chafetz, H. S., Rush, F., & Utech, N. M. (1991). Microenvironmental controls on mineralogy and habit of CaCO<sub>3</sub> precipitates: An example from an active travertine system. *Sedimentology*, 38, 107–126.
- Chafetz, H. S., & Folk, R. L. (1984). Travertine: Depositional morphology and the bacterially constructed constituents. *Journal of Sedimentary Research*, 54, 289–316.
- Collignon, R. (1887). Les ages de la pierre en Tunisie. *Matériaux pour l'Histoire Primitive et Naturelle de l'Homme* [The Stone age in Tunisia materials for natural and primitive human history], 3, 171–204.
- Croci, A. Della, Porta, G., & Capezzuoli, E. (2015). Depositional architecture of a mixed travertine-terigenous system in a fault-controlled continental extensional basin (Messinian, Southern Tuscany, Central Italy). *Sedimentary Geology*, 332, 13–39.
- De Filippis, L., Faccenna, C., Billi, A., Anzalone, E., Brillì, M., Soligo, M., & Tuccimei, P. (2013). Plateau versus fissure ridge travertines from Quaternary geothermal springs of Italy and Turkey: Interactions and feedbacks between fluid discharge, paleoclimate, and tectonics. *Earth-Science Reviews*, 123, 35–52.
- Drysdale, R. N. (1998). Aquatic insect larvae as geomorphic agents in travertine-building: A case study from the Barkly karst, Australia. *Supplementi, Geografia Fisica e Dinamica Quaternaria*, 3, 53–59.
- Drysdale, R. N. (1999). The sedimentological significance of hydropsychid caddis-fly larvae (order; Trichoptera) in a travertine-depositing stream; Louie Creek, Northwest Queensland, Australia. *Journal of Sedimentary Research*, 69, 145–150.
- Drysdale, R. N., Carthew, K. D., & Taylor, M. P. (2003). Larval caddis-fly nets and retreats: A unique biosedimentary paleocurrent indicator for fossil tufa deposits. *Sedimentary Geology*, 161, 207–215.
- Dunham, R. J. (1962). Classification of carbonate rocks according to depositional texture. In W. E. Ham (Ed.), *Classification of Carbonate Rocks* (pp. 108–121). Tulsa, OK: AAPG.
- Edmunds, W. M., Guendouz, A. H., Mamou, A., Moula, A., Shand, P., & Zouari, K. (2003). Groundwater evolution in the Continental Intercalaire aquifer of southern Algeria and Tunisia: Trace element and isotopic indicators. *Applied Geochemistry*, 18, 805–822.
- Embry, A. F., & Klovan, J. E. (1971). A Late Devonian reef tract on northeastern Banks Island, Northwest Territories. *Bulletin of Canadian Petroleum Geology*, 19, 730–781.
- Folk, R. L., & Chafetz, H. S. (1983). Pisoliths (pisoids) in Quaternary travertine of Trivoli, Italy. In T. M. Peryt (Ed.), *Coated Grains* (pp. 474–487). Berlin: Springer.
- Folk, R. L., Chafetz, H. S., & Tiezzi, A. (1985). Bizarre forms of depositional and diagenetic calcite in hot-spring travertine, central Italy. In N. Schneidermann & M. Harris (Eds.), *Carbonate Cements. SEPM Special Publication*, 36 (pp. 349–369). Tulsa, OK: SEPM.
- Ford, T. D., & Pedley, H. M. (1996). A review of tufa and travertine deposits of the world. *Earth-Science Reviews*, 41, 117–175.
- Frizon de Lamotte, D., Saint-Bezar, B., Bracene, R., & Mercier, E. (2000). The two main steps of the Atlas building and geodynamics of the western Mediterranean. *Tectonics*, 19, 740–761.
- Gallala, W., Gaied, M. S., Essefi, E., & Montacer, M. (2010). Pleistocene calcretes from eastern Tunisia: The stratigraphy, the microstructure and the environmental significance. *Journal of African Earth Sciences*, 58, 445–456.
- Gandin, A. & Capezzuoli, E. (2008). Travertine versus Calcareous tufa: Distinctive petrologic features and related stable isotopes signature. *Italian Journal of Quaternary Science*, 21, 125–136.
- Gandin, A., & Capezzuoli, E. (2014). Travertine: Distinctive depositional fabrics of carbonates from thermal spring systems. *Sedimentology*, 61, 264–290.
- Gharbi, M., Bellier, O., Masrouhi, A., & Espurt, N. (2014). Recent spatial and temporal changes in the stress regime along the southern Tunisian Atlas front and the Gulf of Gabes: New insights from fault kinematics analysis and seismic profiles. *Tectonophysics*, 626, 120–136.
- Gobert, G. (1952). El Mekta, station princeps du Capsien. *Karthago*, 3, 1–79.

- Guiraud, R., & Bosworth, W. (1997). Senonian basin inversion and rejuvenation of rifting in Africa and Arabia: Synthesis and implications to plate-scale tectonics. *Tectonophysics*, 282, 39–82.
- Guo, L., & Riding, R. (1998). Hot-spring travertine facies and sequences, Late Pleistocene, Rapolano Terme, Italy. *Sedimentology*, 45, 163–180.
- Guo, L., & Riding, R. (1999). Rapid facies changes in Holocene fissure ridge hot spring travertine, Rapolano Terme, Italy. *Sedimentology*, 46, 1145–1158.
- Hancock, P. L., Chalmers, R. M. L., Altunel, E., & Çakir, Z. (1999). Travertines: Using travertine in active fault studies. *Journal of Structural Geology*, 21, 903–916.
- Henchiri, M. (2014a). Depositional morphotypes and implications of the Quaternary travertine and tufa deposits from along Gafsa Fault: Jebel El Mida, southwestern Tunisia. *Journal of African Earth Sciences*, 90, 9–24.
- Henchiri, M. (2014b). Sedimentology of Quaternary calcareous tufas from Gafsa, southwestern Tunisia. *Arabian Journal of Geosciences*, 7, 2081–2091.
- Hlaïem, A. (1999). Halokinesis and structural evolution of the major features in eastern and southern Tunisian Atlas. *Tectonophysics*, 306(1), 79–95.
- Huerta, P., Armenteros, I., Tomé, O. M., González, P. R., Silva, P. G., González-Aguilera, D., & Carrasco-García, P. (2016). 3-D modelling of a fossil tufa outcrop. The example of La Peña del Manto (Soria, Spain). *Sedimentary Geology*, 333, 130–146.
- Jones, B., & Renaut, R. W. (2008). Cyclic development of large, complex calcite dendrite crystals in the Clinton travertine, Interior British Columbia, Canada. *Sedimentary Geology*, 203, 17–35.
- Jones, B., & Renaut, R. W. (2010). Calcareous spring deposits in continental settings. *Developments in Sedimentology*, 61, 177–224.
- Khatib, S., Rochette, P., Alçiçek, M. C., Lebatard, A. E., Demory, F., & Saos, T. (2014). Etude stratigraphique, sédimentologique et paléomagnétique des travertins de Denizli (Turquie) contenant des restes fossiles quaternaires (Stratigraphic, sedimentological and paleomagnetic study of the Kocabaş travertine, Denizli Basin, Anatolia, Turkey). *Anthropologie*, 118, 16–33.
- Kitano, Y. (1963). Geochemistry of calcareous deposits found in hot springs. *Journal of Earth Science, Nagoya University*, 11, 68–100.
- Koban, C. G., & Schweigert, G. (1993). Microbial origin of travertine fabrics 2 two examples from southern Germany (Pleistocene Stuttgart Travertine and Miocene Riedoschingen Travertine). *Facies*, 29, 251–263.
- Lavigne, F., & Suwa, H. (2004). Contrasts between debris flows, hyperconcentrated flows and steam flows at a channel of Mont Semeru, East Java, Indonesia. *Geomorphology*, 61, 41–58.
- Mannaï-Tayech, B. (2009). The lithostratigraphy of Miocene series from Tunisia, revisited. *Journal of African Earth Sciences*, 54, 53–61.
- Marsily, G. (1981). *Hydrogéologie quantitative*. Paris: Masson.
- Martini, I., & Capezzuoli, E. (2014). Interdigitated fluvial clastic deposits and calcareous tufa testifying an uplift of the catchment area: An example from the Pianizzoli area (southern Tuscany, Italy). *Sedimentary Geology*, 299, 60–73.
- Miall, A. D. (1996). *The Geology of Fluvial Deposits* (p. 582). Berlin: Springer Verlag.
- Nichols, G. (2005). Tertiary alluvial fan at the northern margin of the Ebro Basin: A review. In A. M. Harvey, A. E. Mather, & M. Stoekes (Eds.), *Alluvial fans: Geomorphology, sedimentology, dynamics* Special Publications (pp. 187–206). London: Geological Society.
- Ouda, B., Zouari, K., Ben Oueddou, H., Chkir, N., & Causse, C. (1993). Nouvelles données paléoenvironnementales pour le Quaternaire récent en Tunisie centrale (bassin de Maknassy). *Comptes Rendus de l'Académie des Sciences*, 326, 855–861.
- Pedley, M. (2009). Tufas and travertines of the Mediterranean region: A testing ground for freshwater carbonate concepts and developments. *Sedimentology*, 56, 221–246.
- Pentecost, A. (2005). *Travertine*, (445 pp). Berlin: Springer Science & Business Media.
- Pursell, V. J. (1985). *The petrology and diagenesis of Pleistocene and recent travertine from Gardiner, Montana, and Yellowstone National Park, Wyoming* (Unpubl. M.S. thesis). University of Texas, Austin, TX.
- Regaya, K. (2002). Genèse calcaire associées aux glacis-terrasses de la dorsale tunisienne (piémonts occidentaux de Jebel Bargou) [Limestone genesis associated with Glacis-terrasses of the tunisian ridge (western piedmonts of Jebel Bargou)]. *Notes de service géologique de Tunisie*, 69, 39–51.
- Roche, P. A., & Thiery, M. (1984). Simulation globale de bassin hydrogéologique. Introduction à la modélisation et description du Modèle GARDENIA [Global simulation of hydrogeological basin. Introduction to the modelization and description of GARDENIA model]. *Rapport BRGM*, 84, 337p.
- Saïd, A., Chardon, D., Baby, P., & Ouali, J. (2011). Active oblique ramp faulting in the Southern Tunisian Atlas. *Tectonophysics*, 499, 178–189.
- Selim, H. H., & Yanik, G. (2009). Development of the Cambazlı (Turgutlu/MANISA) fissure ridge-type travertine 744 and relationship with active tectonics, Gediz Graben, Turkey. *Quaternary International*, 199, 157–163.
- Swezey, C. (1997). Climatic and tectonic controls on quaternary eolian sedimentary sequences of the Chott Rharsa basin, southern Tunisia. (PhD. Dissertation), (243p). The University of Texas Houston.
- Vaufrey, R. (1933). Les plissements Acheuléo-Moustériens des alluvions de Gafsa. *L'Anthropologie*, 113, 83–92.
- Viles, H. A., Taylor, M. P., Nicoll, K., & Neumann, S. (2007). Facies evidence of hydroclimatic regime shifts in tufa depositional sequences from the arid Naukluft Mountains, Namibia. *Sedimentary Geology*, 195, 39–53.
- Wentworth, C. K. (1922). A scale of grade and class terms for clastic sediments. *Journal of Geology*, 30, 377–392.
- Zargouni, F., & Ruhland, M. (1981). Style de déformation du Quaternaire récent lié au coulissement de la faille de Gafsa et chronologie des phases tectoniques de l'Atlas méridional tunisien [Deformation style of Late Quaternary linked to the fault of Gafsa and chronology of the tectonic phases of the southern Tunisian Atlas]. *Comptes-Rendus de l'Académie des Sciences*, 292, 913–915.
- Zouari, H., Turki, M. M., & Delteil, J. (1990). Nouvelles données sur l'évolution tectonique de la chaîne de Gafsa [New data on the tectonic evolution of the Gafsa Chain]. *Bulletin de la Société Géologique de France*, 8, 621–628.